Identification and electrophysiological characterization of NpH_V1: a new voltage-gated proton channel

Inaugural dissertation

for the attainment of the title of doctor
in the Faculty of Mathematics and Natural Sciences
at the Heinrich Heine University Düsseldorf

presented by

Gustavo Chaves Barboza
from San José, Costa Rica

Nuremberg, March 2017

from the Institute for Complex Systems - Cellular Biophysics, ICS-4,
at the Forschungszentrum Jülich

Published by permission of the
Faculty of Mathematics and Natural Sciences at
Heinrich Heine University Düsseldorf

Supervisor: Prof. Dr. Christoph Fahlke
Co-supervisor: Prof. Dr. Henrike Heise

Date of the oral examination: 23.08.2017

I declare under oath that I have compiled my dissertation independently and without any undue assistance by third parties under consideration of the “Principles for the Safeguarding of Good Scientific Practice” at Heinrich Heine University Düsseldorf’.

_____ _____

Place, date Signature

Contents

Section *Page*

List of figures

Figure *Page*

List of tables

Table *Page*

List of photographs

Photography *Page*

Zusammenfassung

Der pH-Wert beeinflusst alle Funktion lebender Organismen, aus diesem Grund ist das Proton eines der am stärksten kontrollierten Ionen. Die Regulation des pH-Werts im Zytosol muss sich auf die pH-Änderungen, durch den Stoffwechsel oder Veränderungen des äußeren Milieus einstellen können.

Einige Mechanismen um Protonen zu transportieren sind von der Natur entwickelt worden. Proteine wie der M2 Protonenkanal des Grippevirus, dem Gramicdin Kanal vom *Bacillus Brevis*, die H^+ATPasen, Bakteriorhodopsin, Cytochrom-C-Oxidase in der Mitochondrienmembran und die Carboanhydrase, sowie der spannungsabhängige Protonenkanal transportieren Protonen und verändern die pH-Homöostase.

Bei spannungsabhängigen Ionenkanälen ist der, spannungsabhängige Protonenkanal H_V1 der Einzige, der perfekte Protonenselektivität zeigt. Sein Öffnen ist nicht nur spannungsabhängig, sondern auch pH abhängig, was den Kanal zu einem natürlichen pH-Meter macht und zu einem effektiven Mechanismus um Protonen aus der Zelle zu leiten.
Seit der Entdeckung des Gens für H_V1 im Jahre 2006 wurde jeweils nur ein Gen pro Spezies festgestellt. Obwohl H_V1 im Reich der Tiere stark verbreitet ist, konnte noch kein H_V1 in dessen größter Klasse den Insekten entdeckt werden.

Diese Arbeit ist eine Erstbeschreibung eines spannungsabhängigen Protonenkanals in Insekten. Die detaillierte Untersuchung zeigt, dass der Insektenkanal alle grundsätzlichen biophysikalischen Eigenschaften, mit ein paar interessanten Unterschieden, mit anderen spannungsabhängigen Protonenkanälen teilt. Die Entdeckung dieses Protonenkanals öffnet nicht nur das wissenschaftliche Feld, um eine weitere Klasse von Lebewesen, sondern hilft möglicherweise, die physiologische Bedeutung und die Funktion von spannungsabhängigen Protonenkanälen besser zu verstehen.

Abstract

pH is an important aspect in living organisms and therefore, the proton is one of the most controlled ions. In the cells, pH changes are produced due to their intrinsic metabolism or because of external sources where the efficiency to regulate the proton concentration of the intracellular plasma results essential.

Several mechanisms able to transport protons have been developed by nature. Proteins as the M2 proton channel of influenza virus, the gramidicine channel from *Bacillus brevis*, H^+ - ATPases, the bacteriorhodopsin, the cytochrome c oxidase on the mitochondrial membrane, the carbonic anhydrase and voltage-gated ion channels move protons and modify the pH homeostasis.

Among the voltage-gated ion channels, the voltage-gated proton channel, H_V1, is the only one known which shows perfect selectivity for protons. Its opening is not only voltage dependent but pH dependent as well, which makes it a perfect natural pH-meter and the most efficient mechanism of proton extrusion.

Since the discovery of the H_V1 gene in 2006, only one gene per species has been found and despite to be commonly present along the Animalia kingdom, never founded in its biggest class: the insects.

This work describes for the first time the finding of a voltage-gated proton channel in insects. The detailed electrophysiological characterization shows that the channel has all the determinant biophysical properties of other known voltage-gated proton channels but with some interesting differences. The discovery not only opens the proton channel research to a new class of species but may help to understand H_V1 physiological and functional mechanism better.

To my niece Tamara.

1. Introduction

1.1 Definition and functions

The voltage-gated proton channel, H_V1, is a membrane protein belonging to the family of ion channels that has been found in several eukaryotic cells. Because of its ion channel nature, it conducts proton without ATP consumption and it is electrogenic [1].

The channel is regulated by both the electric potential and the proton gradient across the cell membrane. It opens with a probability that increases with depolarization of the cell membrane and as well when the external pH, pH_o, is increased or when the internal pH, pH_i, decreased. In other words, it works with an electrochemical gradient that result in the channel opening when acid extrusion is favorable.

No systematic nomenclature yet exist for designating proton channels [2]. For example, *HVCN1*, *Hvcn1* and *hvcn1* are gene nomenclatures related with the gene products H_V1 (humans) [3], mVSOP (mouse) [4] and CiVSOP (*Ciona intestinalis*) [4], respectively. Along this document the common form, H_V1, will be used for naming voltage-gated proton channels. Here, H refers to the conducting ion, the proton; the sub-index "$_V$" makes mention to voltage-activation and the number "1" makes reference to the isoform. One or two prefix letters are used for indicating the common name or the genus and species, correspondingly [2].

The channel presents several characteristics, some of them unique, that make it an special case among other ion channels and other proton transporters [5]. Some of its characteristics include: extremely high proton selectivity, voltage-dependent gating, small unitary conductance, absence of saturation, strong temperature dependence

of both conduction and gating, pH-dependent gating and inhibition by some polyvalent cations [2], [5], [6].

In general and under normal conditions, it increases pH_i, decreases pH_o and hyperpolarizes the membrane potential [6]. To date, only one exception has been found in dinoflagellates where proton influx through the channel is presumed to be used for triggering bioluminescence [7], besides of this case, all other studies point out to acid extrusion as its main function.

H_V1 could be found in different kind of cells and its biological function varies depending on them. In humans, H_V1 plays an important role in regulation of pH_o of airway epithelium cells [8]–[10], sperm motility and capacitation [11], [12], charge compensation and ROS production during respiratory burst of phagocytes [13]–[22], B cells signaling [21], histamine release by basophils [23], proton extrusion during action potentials in skeletal muscle myotubes [22], regulation of cytosolic pH in osteoclasts [24], regulation of insulin secretion by pancreatic islet β-cells [25], among others.

But expression of H_V1 is not in all the cases positive for health. For instance it has been related with excessive ROS production in microglia [26], [27] which worsen pathologies of ischemic stroke, Parkinson's disease, aging, atherosclerosis, Alzheimer and ischemic liver disease [6]. As well, it has been linked to malignant B cells in patient suffering of lymphocytic leukemia [28], metastasis of breast cancer cells [29], [30], colorectal cancer [31] and recently found in human glioblastoma multiforme cells, "the most common and lethal brain tumor" [32].

Under this context, the voltage-gated proton channel starts to become an attractive target for therapeutic approaches [33]–[37] or to other applications like biofuels [38].

1.2 History and background

H_V1 was firstly identified by Thomas and Meech in 1982 in *Helix aspersa* snail neurons, when proton currents during membrane depolarization were detected [39]. Ten years before, the idea of the existence of a proton conducting entity related with bioluminescence triggering in dinoflagellates was hypothesized by Fogel and Hastings [40] but never proved.

In 1984, Byerly *et al.* [41] described the electrophysiological properties of H_V1 in the snail *Lymnaea stagnalis*, work that helped to consider the proton channel as special among other ion channels. Further, the same year Barish and Baud found voltage-gated proton currents in newt oocytes from the species *Ambystoma* [42].

For several years, there were no further publications about voltage-gated proton channels. However in 1991, the channel was identified for the first time in mammalian cells by DeCoursey [43] and two years later discovered in humans [17], [44]. Afterwards, the number of H_V1 publications increased to summed up close to hundred voltage-clamp studies and reviews up to 2003 [5].

A breakthrough took place in 2006 when the H_V1 gene was discovered in humans, mouse and the ascidian *Ciona intestinallis* [3], [4]. Knowing the codifying sequence for proton channels facilitated further studies related with structure and functional mechanism of the channel.

Hence, in 2008 the protein was reported to have a dimeric nature [45]–[47] and the knockout mouse model developed afterwards [14], [15], [48]. In 2011 the amino acid responsible for the perfect selectivity was found by Musset *et al.* [49] and the hypothesis of proton channels in dinoflagellates confirmed [7]; meanwhile finally in 2014 the first and up to date the only H_V1 crystal structure, came out [50].

Nowadays, around 350 direct and/or peripheral voltage-clamp studies among scientific papers, reviews and Ph.D. dissertations, can been found (*Source: Personal communication with T.E. DeCoursey)*.

Figure 1.1 exhibits a timeline of the development of the proton channel field from 1982 until now.

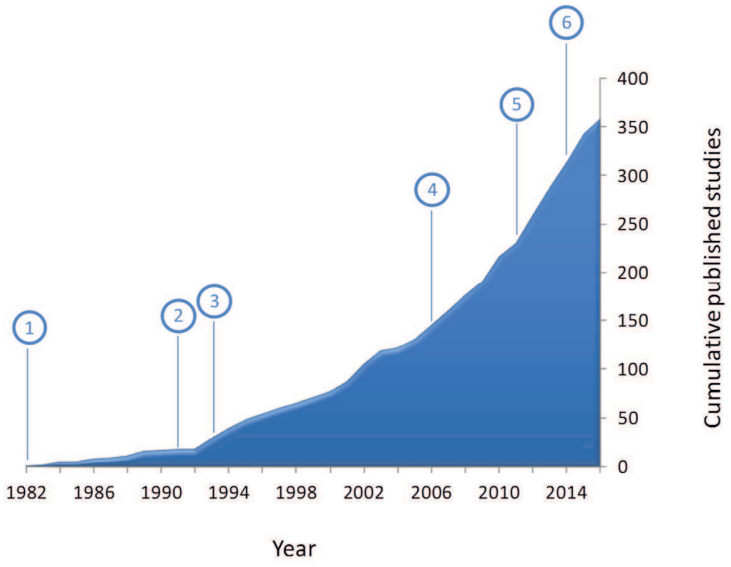

Figure 1.1. **Voltage-clamp studies of H_V1.** Timeline showing the cumulative number of publications to date. Some remarkable discoveries are numbered as follows: 1) First report of H_V1 in snail neurons; 2) H_V1 detection in mammalian cells; 3) First description in human cells; 4) The H_V1 gene is elucidated; 5) The selectivity filter is identified in the human protein; 6) First X-ray structure resolved. *Data kindly provided by T.E. DeCoursey.*

1.3 Structural insights

General structure

In humans, H_V1 is described as a protein composed of 273 amino acids (31.7 kDa, pI = 6.62) [3]. It is formed by four transmembrane segments, conventionally named as S1, S2, S3 and S4. These segments consist in four alpha helix joined together by three short linkers with high homology in the S2-S3 linker among proton channels [2]. The amino and carboxyl terminal domains of the channel are located in the intracellular space (**Figure 1.2**).

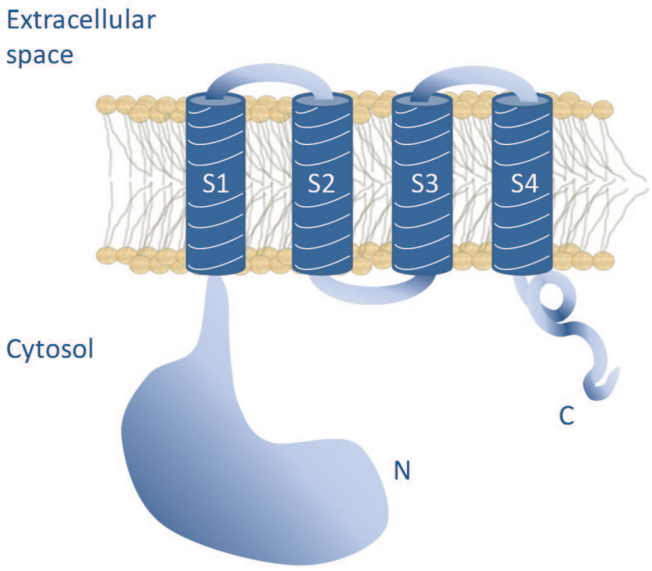

Figure 1.2. **Representation of the general structure of H_V1.** S1-S4 represent the four transmembrane segments; the amino and carboxyl terminal domains are labeled as N and C, respectively.

When compared with other voltage-gated ion channels like sodium, potassium or calcium, H_V1 lacks of the S5 and S6 segments that forms the pore in those proteins

but keeps high homology with their voltage-sensing domain (VSD) [3], [4], [51]. Because of this, H_V1 has been called as well "voltage-sensor domain only protein" (VSOP) [4], [13], [52], [53]. As well, it has a high resemblance with S1-S4 regions of voltage sensing phophatases (VSP) [4]. (*See* **Figure 1.3**)

It exist strong evidence pointing out to the existence of H_V1 as a dimer, at least when it is expressed in a heterologous system [45]–[47]. Here the C-terminus plays an important role and is generally accepted that interactions due to its coiled-coil topology holds the dimer together, statement supported by several studies [45]–[47], [54], [55] and confirmed via crystal structure of the single domain [56]. The biophysical consequence of H_V1 oligomerization is an enhancement of the voltage-dependence of activation and decrease of gating kinetics [57].

In the H_V1 dimer, each of the monomers is considered proton conductive [46], [47], [54], preserving most of the main biophysical properties [55].

The dimeric existence of H_V1 has been attributed to humans (hH_V1), mouse (mVSOP) and *Ciona intestinalis* (CiH_V1), all of them vertebrates. However, it seems that proton channels from the invertebrates *Karlodinium veneficum* (kH_V1) and *Phaeodactylum tricornutum* (PtH_V1), consist in monomers and not in dimers [2]. The conclusion has arrived based on the lacking of a predicted coiled-coil in C-terminus, an important feature in the interaction of both subunits. In addition, kH_V1 presents weak Zn^{2+} inhibition and exponential activation [7], both characteristics of monomeric proton channels [54].

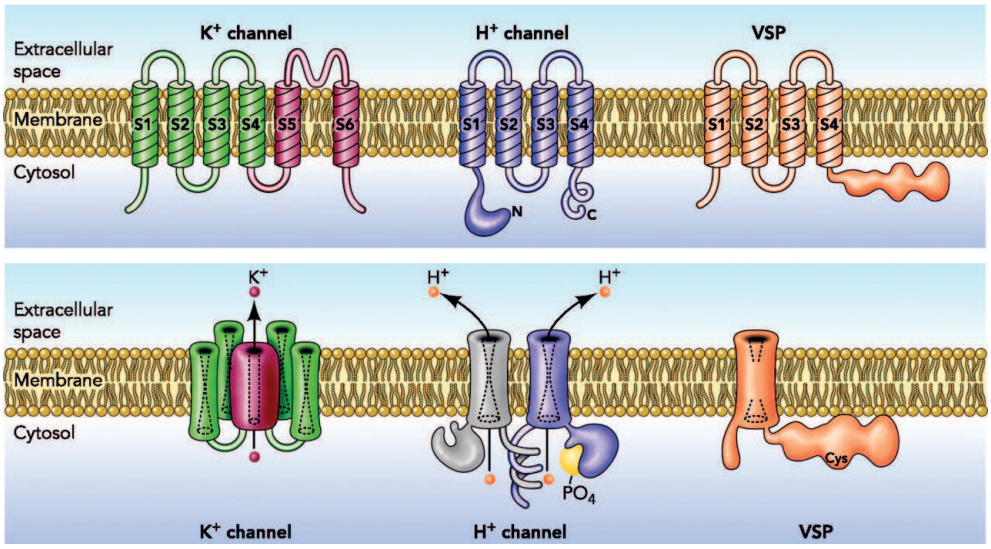

Figure 1.3. **Structural comparisons of H_V1 and other similar proteins.** The upper row shows the monomers for voltage-gated K^+ channels, proton channels and voltage-sensing phosphatases. The lower row presents the final oligomers. H_V1 is a dimer held together by interaction of a coiled-coil in the C-terminus where each monomer is proton conducting. *Figure taken from*[58].

The N-terminus is necessary for an "enhanced gating mode" which results in activation at more negative voltages [59]. As well, it seems possible that it contributes to oligomerization [47] [2]. In humans, the N-terminus has reported a length of approximately 100 amino acids, showing high homology to protein and lipid phosphatases [3].

Up to date, a single crystal structure is known for H_V1. It consist in a chimeric mouse H_V1 where the N-terminus was removed, the region from the middle of S2 to the middle of S3 replaced with its homologous region from *Ciona instestinalis* voltage-sensing phosphatase (Ci-VSP) and the C-terminal coiled-coil replaced with a leucine-zipper motif of a transcriptional activator from *Saccharomyces cerevisiae* [50]. Yet, with the exception of faster gating, all main electrophysiological characteristics of H_V1 are preserved [6]. Since there's no membrane potential or pH gradient in a

crystal, and because H_V1 opens at positive voltages when $pH_o = pH_i$, this structure seems to correspond to the close state [6].

Voltage sensor

The voltage sensor domain (VSD) of voltage-gated ion channels is composed by a region with high homology in function and structure. As it has been mentioned before, transmembrane segments S1-S4 are considered homologous to the VSD of potassium, calcium and sodium channels. In this family of channels, is generally accepted that the voltage sensing relies on positive charged amino acids distributed along the fourth transmembrane segment (S4) of the domain [51] (**Figure 1.4**)

Figure 1.4. **Positive charges are consistent along S4 segment of voltage-sensing domains.** Above: Alignment of S4 segment of H_V1 in *Homo sapiens* (hH_V1), *Mus musculus* (mVSOP), *Gallus gallus* (ChH_V1), *Danio rerio* ($DanH_V1$), *Ciona intestinalis*(CiH_V1) and *Karlodinium veneficum* (kH_V1). Below: Alignment of S4 segment from domain IV of $Na_V1.4$, $K_V1.2$ and *Shaker* K. Positive residues are highlighted in blue. R1, R2 and R3 located in the middle of the segment (shaded) are well conserved in all cases.

In the case of the S4 in H_V1, a pattern of three arginine residues R1, R2 and R3, separated by two hydrophobic residues is well conserved among proton channels

and is considered responsible for voltage sensing [51], [60]–[63]. Even more, the mentioned pattern, RxWRxxR, is considered a "signature sequence" of H_V1 and has been used before as a tool for detecting them [2], [7], [64].

Several studies proposed that during depolarization three arginine residues in S4, R1, R2 and R3, sense the voltage and cause an helical screw movement of the segment [61], [65]–[68]. Neutralization of any of those charged amino acids reduces the voltage dependence of activation [66]. The S4 voltage-dependent movement brings a subsequent channel's open configuration where an additional movement of S1 segment during conduction has been proposed [68], [69].

The channel opening is considered slow and strongly regulated by dimerization. The gating charge for the dimer is reported as 5.9 e_0 and as 2.7 e_0 for the monomer [65], [70].

The open state and the selectivity filter

There is no crystal structure of the open state. However, there are different computational models based on experimental data describing important aspects as the proton pathway, the selectivity mechanism and gating [61], [67]–[69], [71]–[73].

Research on classical voltage-dependent ion channels has brought some important clues about the proton permeation pathway. For example, studies with *Shaker* K^+ proved the existence of a constriction similar to an hour glass of water molecules in its VSD (S1-S4) [74]. As mentioned in the previous section, the VSD from the *Shaker* K^+ and other voltage-gated ion channels present close homology with H_V1 (**Figure 1.4**). In S4 from the *Shaker* K^+, R1 is kept retracted toward the constriction in the close state [75]; meanwhile R4 moves upward to the constriction in the open state during depolarization [76] (*see arginine residues in* **Figure 1.4**). It is a hallmark of voltage-gated ion channels that they undergo a conformational change in their VSD previously to channel opening [77]. In the case of the *Shaker* K^+, no ionic currents

flow through the VSD neither in the open state nor in the close state [2], indicating just the voltage sensing phenomena that would open the pore (S5-S6) afterwards. Arg to His mutations done by Starace *et al* in the S4 segment of a non-conducting *Shaker* K^+ resulted in the appearance of proton selective currents, concluding that the substitutions allow the VSD to transport protons [78] and that protons from internal and external solutions are separated by a narrow barrier that focuses the electric field [75]. In that way, a K^+ channel becomes a H^+ channel once the constriction has an amino acid that enables protonation in one side and deprotonation in the other side. Studies of other proteins as $Na_V1.4$ from skeletal muscle, the M_2 influenza channel and human carbonic anhydrase II, show His facilitated proton transfer [2].

Among proton transfer pathways, the Grotthuss mechanism is considered the main mechanism of H^+ conduction in water [1]. In Grotthuss mechanism, a proton binds to a neighboring water molecule to form a hydronium ion. Afterwards, that hydronium will lose any of the three protons which will be accepted by the nearest and favorable oriented water molecule [1]. The mechanism allows protons to travel faster than other ions which have hydratation shell while moving through the water. In the proton channel field, water wires, a single file of waters aligned in a very narrow and hydrophobic region, have been proposed for some researchers as an essential part of the conduction pathway [72]. However, several facts as high H^+ current reduction in D_2O, high temperature dependence of H^+ conductance and high proton selectivity indicate that proton conduction in H_V1 is more complex than a simple water wire conduction [5].

H_V1 permeation pathway is better explained on the basis that proton conduction in H_V1 happens accordingly with the hydrogen-bonded chain (HBC) theory from Nagle and Morowitz [79] (**Figure 1.5**) where if at least one of the elements belonging to the HBC is a titratable group, proton selective conduction could be achieved. Hence proton selectivity in H_V1 needs a titratable group, e.g. carboxyl group, which faces the pore in a narrow hydrophobic region.

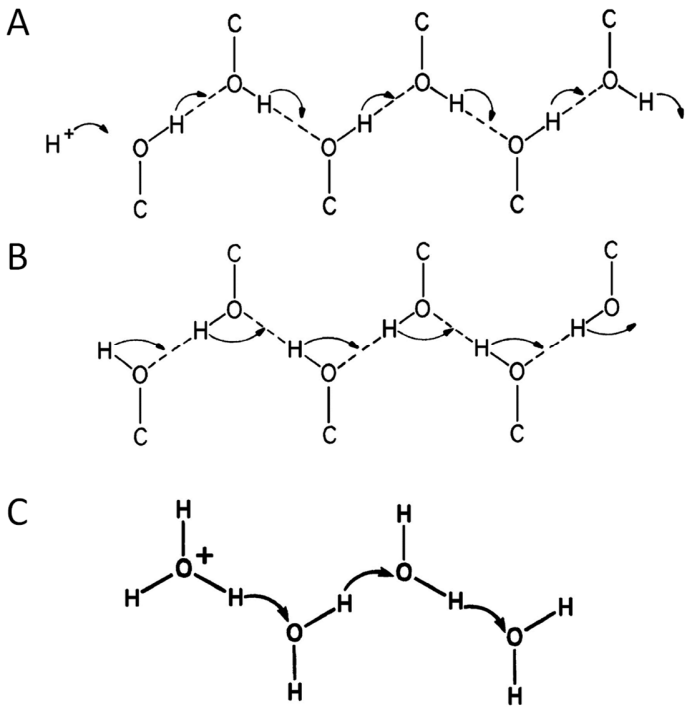

Figure 1.5. **Hydrogen bond chain mechanism, HBC.** A) A proton in the left side binds to the electronegative oxygen of a hydroxyl group causing a proton hopping chain effect, illustrated by the arrows, that end up in the transfer of a proton in the right side. B) The orientation of the HBC changes once the hopping process is completed and a rearrangement of the hydroxyl groups, described by arrows, must be done before allowing transference of other proton. C) Proton conduction in a simple water wire among neighboring water molecules. *Figure taken from* [5]

In this sense, electrophysiological studies have proved that Asp112 and Asp51 are essential for proton selectivity in hH_V1 and in kH_V1, respectively [7], [49]. Both negatively charged residues are analogous and located at the middle of S1 in a bottle neck region. When Asp is exchanged by the also negative Glu, the channel behaves as wild type with the only exception of altering the gating kinetics [2]. On the other hand, its neutralization results in loss of proton selectivity, transforming the proton channel to an anion permeable channel [7], [49]. The aspartate in the middle of S1 is conserved among all known H_V1 [2] and is considered the selectivity filter [2]. In a

selectivity filter scanning of the human channel, Morgan *et al* mutated Asp112 to Ala and introduced Asp in every single position along S1, from 108 to 118. Moving the Asp to other positions than 116 resulted in loss of proton selectivity Proton selective conduction was only restored when Val116 was mutated to Asp or Glu [73]. Their results not only confirm the importance of a negative residue facing the pore of the channel but delimitate the local environment necessary for proton selective conductance as well.

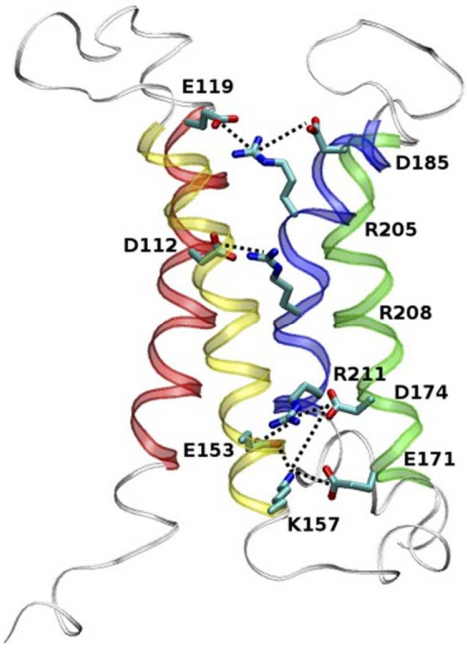

Figure 1.6. **Putative open state of the human voltage-gated proton channel.** Transmembrane segments are color-labeled: S1, red; S2, yellow; S3, green and S4, blue. The extracellular space is located at the top meanwhile the intracellular one at the bottom. Charged amino acids are labeled and salt bridge interactions between them represented by pointed lines. D112 is vital for proton selectivity and it interacts with the second arginine in S4. Structure of R2D homology model proposed by Kulleperuma *et al.* [71].

In most of the homology models proposed, Asp112 or equivalent interacts via salt bridge with one of the argenine residues of S4 [54], [68], [71]–[73] compensating in this way the aspartate negative charge [6] (**Figure 1.6**). The Asp – Arg interaction is important in the selectivity mechanism because according with quantum simulations, it creates an energetic barrier that only protons are able to break [80]. Nonetheless, it exists an open discussion about two possible models depending on which Arg interacts with the Asp, if R2 or R3.

Other significant amino acids

Functions of other amino acids have been identified:

In the N-terminus, Met91 and Thr29 of hH_V1 have been related with gating functions. In activated phagocytes, phosphorylation of Thr29 shifts the g_H-V relationship negatively, conducing to an "enhanced gating" of the channel [59]. This amino acid is conserved among species with the exceptions of *Strongylocentrotus, Nicoletia* [64], *Karlodinium* and *Ciona* [2]. On the other side, M91T is attributed to a natural occurring mutation which alters the threshold potential, V_{thres}, at any given proton gradient [81].

In hH_V1, His140 and His193 are located in S2 and S3-S4 linker, respectively. Both residues contribute to zinc sensitivity [54]. In the case of His193, the residue is found in mammals and birds, but substituted by Asp or Glu in aquatic species, with the exception of *Nematostella* where Asn can be found at the same position [2].

Phe150 in hH_V1 is conserved among VSD [82]. It is located in S2 and has been described as the outer limit of the charge transfer center or hydrophobic gasket in K^+ channels [83]. Together with other two hydrophobic residues, Val109 and Val178, could forms an hydrophobic region that focus the electrical field and which S4 argenines pass by in their movement due to depolarization [82].

A tryptophan in the middle of S4, just next to R2, is well conserved among proton channels (**Figure 1.4**) and forms part of the characteristic signature sequence RxWRxxR. Into this signature sequence, Tryp207 determinates the properties of hH_V1 as slow channel opening, proton selectivity, ΔpH-dependent gating and highly temperature-dependent gating kinetics [84].

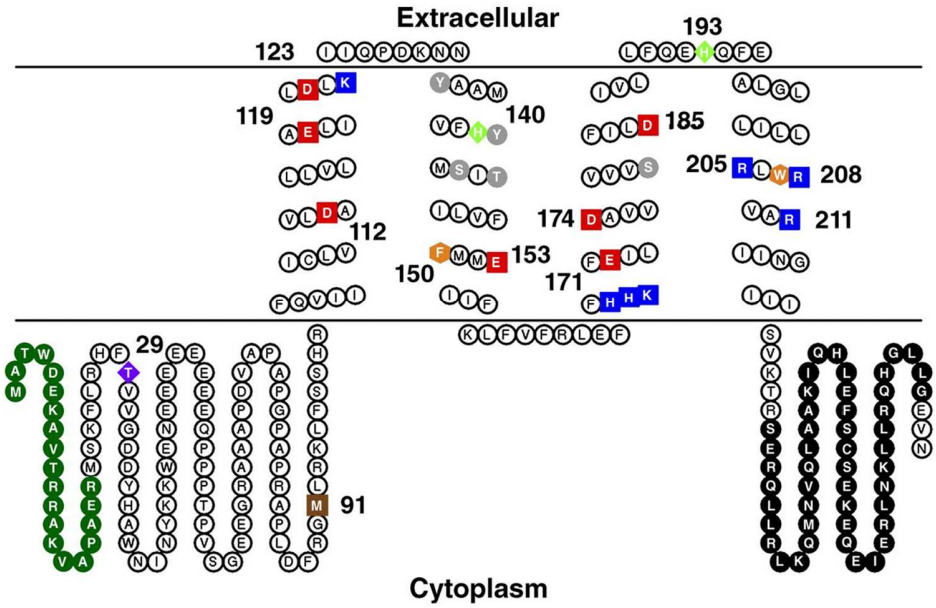

Figure 1.7. **Schematic structure and amino acid sequence of hH_V1**. In the transmembrane segments: basic residues in blue, acidic residues in red, aromatic residues in orange and polar residues in grey. Other residues which specific functions have been identified: Deletion of green amino acids in N-terminus (1-20) are absent in a short isoform common in malignant B cells [28]; phosphorylation of Thr29 produces an enhanced mode [59]; Met91 is the first natural mutation present in hH_V1 [81]; Asp112 is crucial for proton selectivity [49]; His140 and His193 are the Zn^{2+} binding sites between the monomers [3], [54]; Arg205, Arg208 and Arg211 for the putative voltage sensing domain; the C-terminus forms a coiled-coil that hold the dimer together [45]–[47]. *Figure taken from* [82].

Negative residues in S2 and S3 are thought to serve as counter charges of the positives residues in S4 [2], stabilizing in this way the closed state. The statement is

in agreement with Ramsey *et al* study of hH_V1 where neutralization of Glu153(in S2) and Asp174 (in S3) shifted the g_H – V curve negatively [85].

Figure 1.7 shows a schematic representation of the human H_V1 where it is possible to see the location of the residues described along this section.

1.4 Biophysical properties

Small unitary conductance

The unitary conductance of the voltage-gated proton channel is considered small when compared with other ion channels, 3 orders of magnitude smaller, basically because of the H^+ concentration inside most of cells is $\sim 10^5$ times less than Na^+ and 10^6 less than K^+ [5].

In their study about properties of H_V1 in human eosinophils, Cherny *et al*. report single channel currents of 7 – 16 fA near to the voltage where proton currents activate, known as threshold potential (V_{thres}) [86]. In addition, current variance analysis detected variances of 100 fold or more than background signal where the single channel conductance increase when pH_i decreased, independently of pH_o, [2]. Because the unitary conductance is affected by the pH_i but not by pH_o, it is thought that the conduction ion is H^+ and not OH^- [2].

Single channel conductance for H_V1 is refered as 38 fS at pH_i 6.5, at a maximal open probability P_{open} of 0.75, and 139 fS at pH_i 5.5 with a maximal P_{open} of 0.95 [86]. Extrapolation of these values to physiological pH_i 7.2 gives a conductance of 15 fS at 20 °C and 78 fS at 37 °C [86].

Perfect selectivity

The selectivity of H_V1 (i.e. specificity for protons) has been called a "defining property" and even considered "perfect" [2].

In an open configuration, each channel allows to pass up to 10^5 $H^+ \cdot s^{-1}$ but neither protons nor any other ion permeates once it closes [63].

The relative permeability of H^+ to K^+ could be calculated with the Goldman-Hodgkin-Katz equation, GHK (**Equation 1.1**). Because under physiological conditions the concentrations for potassium and protons are 155 mM and 60 nM respectively, then in the case where K^+ permeability would be the same of H^+, a proton would be conducted every million of potassium ions. This would bring a conductance reversing closer to E_K than to E_H. In all H_V1 studies V_{rev} is $\sim E_H$ and therefore, P_H / P_K should be in at least equal to 10^6.

$$V_{rev} = \frac{RT}{zF} \log\left(\frac{P_{Cl^-}[Cl^-]_i + P_{K^+}[K^+]_o + P_{Na^+}[Na^+]_o + P_{H^+}[H^+]_o}{P_{Cl^-}[Cl^-]_o + P_{K^+}[K^+]_i + P_{Na^+}[Na^+]_i + P_{H^+}[H^+]_i}\right)$$

(Equation 1.1)

where:

V_{rev} = reversal potential
R = gases constant
T = temperature in K
z = charge of the ion
F = Faraday´s constant
P_x = permeability of ion "X"
$[X]_I$ and $[X]_o$ = molar concentration of ion "X" inside and outside, respectively

The selectivity can be evaluated by measuring the V_{rev} in solutions with different ions and compare the result with the Nernst potential for protons (**Equation 1.2**). In

this way, deviations of V_{rev} from E_H can be calculated with GHK and selectivity of the channel defined.

$$E_H = \frac{RT}{zF} \log\left(\frac{[H^+]_o}{[H^+]_i}\right)$$

(Equation 1.2)

where:

E_H = Nernst potential for protons
R = gases constant
T = temperature in K
z = charge of the ion
F = Faraday´s constant
$[H^+]_i$ and $[H^+]_o$ = molar concentration of protons inside and outside, respectively

As matter of comparison with other ion channels, Na^+ channels present P_K/P_{Na} values of 0.05-0.1 and up to 0.23-0.30 (when K^+ is inside and Na^+ outside the cell) and the more selective K^+ channels show P_{Na}/P_K values around 0.001-0.1 [63]. Other ion channels as Cl^- channels have reported still less selectivity, conducting even large organic ions [63].

The assumption that proton relative permeability is at least 10^6 based on ion concentration differences under physiological conditions is supported by several studies and in fact is considered much higher [2], [16], [19], [87]–[89].

For example, a relative proton permeability P_{D_2O}/P_{TMA} as high as 2 x 10^8 in deuterium solutions (pD = 7.0) has been calculated [90]. As well, in all studies done there's no evidence of permeation of any other ion [63] and V_{rev} doesn't change detectably when the predominant cation or anion in the solution is changed, once liquid junction potential differences are corrected [5]. In H_V1 studies, deviations of

V_{rev} from E_H increase with ΔpH, independently of the absolute pH, nonetheless are attributed to imperfect pH control rather than selectivity for other ions [5].

In addition, the use of Barry's strategy to distinguish between cation or anion permeability [91] does not produce changes in V_{rev} once the ionic strength of other ions different than H^+ is reduced to 90 % [49].

Together with electrostatic effects, steric factors play an important role in selectivity. Neither Na^+ (similar size than H_3O^+) [80], [88], nor H_3O^+ [90], [92] or bigger hydratated hydronium forms as $H_5O_2^+$ (Zundel) or $H_9O_4^+$ (Eigen) permeate through H_V1 [6], maybe because protons are much smaller and they don't need an hydratation shell for travel: they can do it just hopping from one ligand to another [6].

The Nernst potential for OH^- is equal to that for protons, however studies suggest OH^- doesn´t permeate. When pH_i is decreased, $[OH^-]_i$ is reduced. This condition creates an outward proton gradient but at the same time and inward hydroxyl gradient, where it is impossible to differentiate which one is the conducting ion via Nernst equation. In this situation, both the proton gradient and the hydroxyl gradient are the same. Nevertheless, in a deuterium isotope effect on permeation from DeCoursey and Cherny [90], it was proved that H^+ and not OH^- is the charge-carrying ion. Since D^+ has a mass twice than H^+ and because OD^- has a mass just 6 % larger than OH^- [90], a meaningful conductance reduction could be expected if H^+ would be the conducting ion due to its mass difference. On the other hand, a smallest effect would be appreciated if OH^- is the conducting species. The results showed a significant conductance reduction in D_2O: the isotope effect for D^+ was reported as 41 % meanwhile the one for OD^- was 3% [90].
Patch-clamp measurements indicate that the amplitude of the currents increase when pH_i is decreased, explained as a consequence of a increment in $[H^+]_i$ and therefore in the electrochemical force. The current increase is considered however, less than proportional to the change in proton concentration [5]. Permeation of OH^-

has been proved as well in hH_V1 by means of sucrose ionic strength dilution, where selectivity for H^+ and not OH^- was confirmed [49].

The extremely high selectivity of H_V1 and the existent evidence are congruent with the assumption that the conduction pathway in the channel is a HBC mechanism which only allows H^+ to pass through [1], [2], [5].

Voltage-dependent gating

H_V1 presents a gating that is regulated by the electric potential across the cellular membrane, however not exclusively. As it will be discussed later, the channel adjusts the gating accordingly with the pH gradient across the membrane (ΔpH) as well.

As most of voltage-gated ion channels, H_V1 opens with a probability that depends on the voltage potential across the cell membrane describing sigmoidal function when is determined as proton conductance g_H [6].

Under symmetrical pH conditions, pH_i / pH_o = 1, H_V1 remains closed at negative voltages and opens at positive ones, conducting proton currents that can be detected at voltage values as high as + 380 mV (**Figure 1.8**) [5]. During depolarization, currents do not saturate as in other ion channels and instead, present a monotonic behavior (**Figure 1.8 B**). Higher depolarization causes an increment of H^+ currents and on the speed of activation kinetics.

Once the channel opens, outward proton currents can be detected during membrane depolarization, describing a "sigmoid activation time course which can be accommodated by introducing an initial delay" [5].

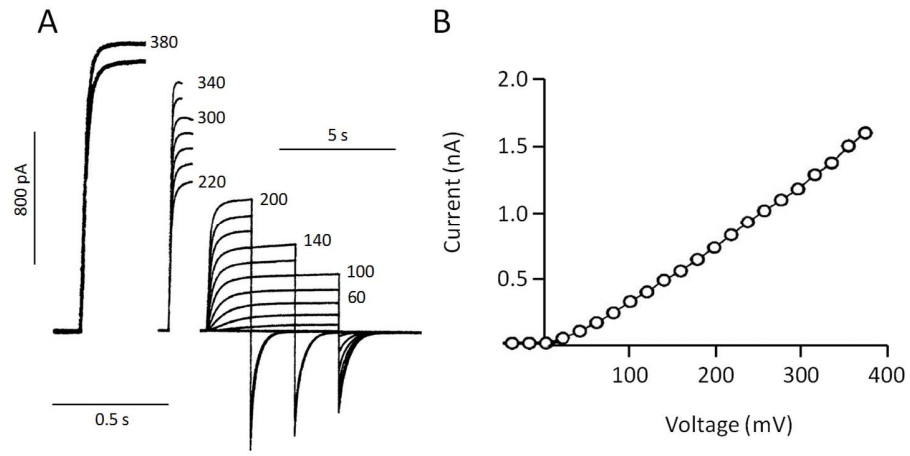

Figure 1.8. **Proton currents show absence of saturation.** A) H^+ currents of a stimulated human eosinophil obtained by means of depolarizing pulses from – 60 mV up to + 380 mV, at $pH_i = pH_o = 7.0$. Pulses were applied in 20 mV steps and the pulse duration reduced for avoiding proton depletion at high voltages. B) Current-voltage relationship from the data in A where there's no evidence of current saturation. *Taken and adapted from* [5].

Sigmoidal activation and the later slow rising of H^+ currents have been attributed to the dimeric nature of proton channels and are considered evidence of cooperative gating between the subunits [54]. In contrast, monomeric H_V1 have demonstrated to activate exponentially and more rapidly [54]. For proton channels, the gating charge calculated by the limiting slope method is reported as 5.9 e_0 for the dimmer and 2.7 e_0 for the monomer [65], suggesting that all the three arginines in S4 contribute to the measured gating charges [51] and that both protomers must open before either can conduct [2].

The activation kinetics are commonly fitted with a single exponential function after a short delay, allowing the estimation of a maximal proton current and a time constant (τ_{act}) at the corresponding voltage pulse (**Figure 1.9**). τ_{act} is the time course of the increase of current during a depolarizing pulse and it's useful to compare the speed of opening of the channel [1].

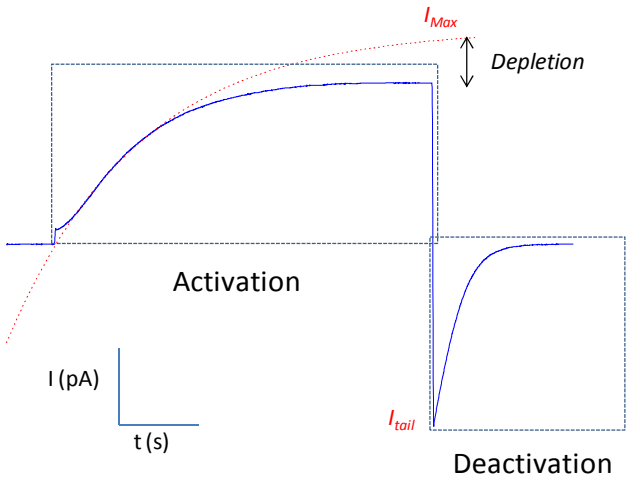

Figure 1.9. **Characteristic proton current signal during depolarization and repolarization of the membrane in whole-cell patch clamp configuration.** Activation kinetics despites a proton outward flux that can be fitted with a single exponential after a short delay (dotted curve). Current droop is considered an effect of depletion of protonated buffer. Deactivation kinetics describes a tail current once the membrane is hyperpolarized that perfectly fits with a single exponential.

Theoretically, H_V1 can effectively either extrude protons or allow them to enter. Thus, when the membrane is repolarized at voltages under the threshold of activation, the channel is forced to close and inward proton currents are observable. H^+ inward currents are possible due to the fact that the process need a time lapse or deactivation phase. The result is the appearance of a deactivating current or "tail current" (**Figure 1.9**) that can be perfectly fitted with a single exponential equation and as in the case of activation kinetics, determined as time constant (τ_{tail}). In H_V1, τ_{act} is voltage and pH dependent, meanwhile τ_{tail} shows only voltage dependence at potentials well negative to V_{rev} [93].

H_V1 closes just after depolarization (deactivation) but never during a depolarizing pulse (inactivation) [1]. Proton channels do not inactivate [1], [5] and current

droops compared with maximal values are considered a consequence of depletion of protonated buffer [1], [5], [43].

The voltage threshold of activation (V_{thres}) or "the voltage where the channel first opens" [1] is estimated by direct observation of typical activation and deactivation kinetics during depolarization and reporalization of the membrane, respectively (**Figure 1.10**), and changes in a reason of ~ 40 mV to more positive or negative voltages once ΔpH changes in one unit [93].

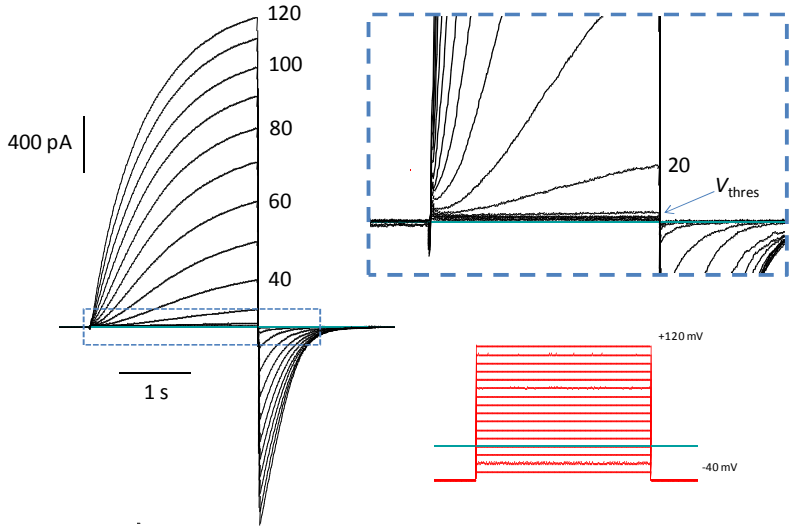

Figure 1.10. ***V*thres direct determination through a family of pulses.** Family of pulses showing a V_{thres} of approximately + 10 mV under symmetrical pH conditions, pH_i = 6.5 and pH_o = 6.5, in a HEK293 cell transfected with hH_V1 WT. Pulses applied in 10 mV increments from – 40 mV to + 120 mV. Pointed frame shows a close up of the region where it is possible to identify V_{thres}.

High temperature dependence

The temperature dependence of a specific property can be measured by the temperature coefficient (Q_{10}), this is, the change in the magnitude of a property once

the temperature is increased 10 ° C. It is a measure of the activation energy (E_a) of a process [1] and can be calculated accordingly with **Equation 1.3** and **Equation 1.4**.

$$Q_{10} = \left(\frac{X_2}{X_1}\right)^{\frac{10}{(T_2 - T_1)}}$$

(Equation 1.3)

$$E_a = \frac{R\ ln(Q_{10})}{\left(\frac{1}{T_1} - \frac{1}{T_2}\right)}$$

(Equation 1.4)

Where:

X_1, X_2 = measured values in state 1 and in state 2, respectively.
T_1, T_2 = temperature of the state 1 and 2 (in Kelvin), respectively.
R = gas constant, 8.314 kJ·mol-1.

The temperature dependence of H_V1 is considered high [1], [62], [92] and one of the most pronounced among ion channels [1].

Q_{10} of proton conductance has been estimated between 2 and 3 along a wide range of cells and species [2], where increments at lower temperatures were detected, for instance up to 5.3 at < 20 °C in excised patches [92]. This value exceeds the range of 1.18 to 1.7estimated for voltage-gated potassium channels and sodium channels [1]. The Q_{10} of proton conductance has been taken as evidence that the conduction pathway in H_V1 is not a water wire, that the process includes one or more tritable groups, and that the rate-limiting step occurs during permeation [2]

The gating kinetics show even more temperature dependence. τ_{act} and τ_{tail} have Q_{10} values on the range of 6-9 [92], meanwhile gating process for most of other ion channels present a Q_{10} of ~3 [2]. In addition, a C-terminus truncated hH_V1 that

carries to channel's monomerization, has demonstrated to have a Q_{10} in the gating kinetics of half of the characteristic one for the dimer, a strong prove of cooperative gating of the dimer subunits [54].

ΔpH-dependent gating

Gating of H_V1 is not only regulated by the membrane potential but as well strongly by the pH gradient across the cell membrane, this means, gating is dependent of the permeant ion concentration [2]. This characteristic is unique among classical voltage-gated ion channels and is considered determinant for the channel's main function: to eliminate intracellular proton excess.

In a detailed study in rat alveolar ephitelial cells, Cherny *et al.* [93] determined the shift produced in the g_H – V curve when pH at both sides of the membrane is altered. They concluded that a shift of 40 mV is produced once the pH gradient across the membrane is changed in one unit, independently of the pH_i or pH_o absolute values [93] (**Figure 1.11**). The shift can be taken then as a change in V_{thres} and calculated using Equation 1.5 [93].

$$V_{thres} = 20 - 40\ \Delta pH\ mV$$

(Equation 1.5)

In a subsequent study using the same kind of cells, DeCoursey and Cherny [90] establish a general equation (**Equation 1.6**) on the basis that ΔpH is better defined by the observable V_{rev} [5]. This method allows evading the problem related with poor pH control during measurements which alter both V_{rev} and gating.

$$V_{\text{thres}} = 0.76\, V_{\text{rev}} + 18\, mV$$

(Equation 1.6)

In Cherny and DeCoursey experiments, the relationships between V_{thres} and ΔpH were kept along a wide range of pH (pH_i 5.5 – 7.5 and pH_o 6 – 8) but with an apparent saturation at pH_o > 8, indicating a pH_o close to the pK_a of an external regulatory protonation residue [93]. Similar saturations have been described in other species and even some studies present an apparent saturation of V_{thres}, which all together could indicate that it consist in a phenomena due to the inability to controlling pH accurately [5].

The 40 mV / ΔpH shift rule has an important physiological implication. The peculiar pH sensitivity of the voltage-dependent gating of H_V1 implies an activation of the channel positive to V_{rev}. Thus, considering that the driving force is described in the Hodgkin and Huxley model [94] as (E_m – E_H), it means that the channel opens only when the electrochemical gradient allows outward proton currents [62] [63], resulting in acid extrusion.

Protonation of an external site promotes a channel closed conformation; meanwhile protonation of an internal site stabilizes the open configuration [93]. With the purpose of revealing the responsible(s) of pH-dependent gating, Ramsey *et al.* [85] neutralized a considerable number of amino acids looking forward to find one or several tritable groups linked to the behavior but in all of them, the 40 mV shift in the g_H – V curve demonstrated to be consistent [85]. Thus far, how H_V1 sense the pH and adjust its gating based on it is still an enigma and it is perhaps, the most important question [6].

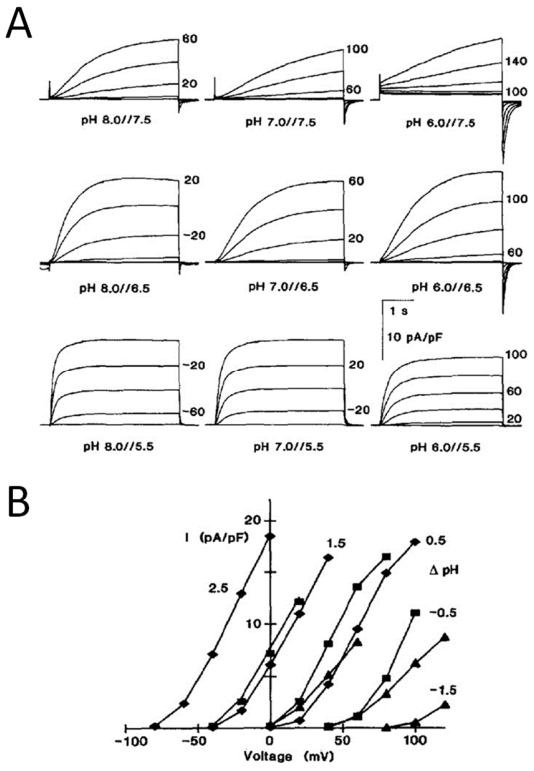

Figure 1.11. **pH-dependent gating of proton currents in the rat alveolar studies of Cherny and DeCoursey** [93]. A) Families of pulses at different pH conditions represented as $pH_o//pH_i$ where it is possible to appreciate how the channel adjust its activation based on ΔpH. Depolarizing pulses where applied in 20 mV increments. B) I-V curve for families shown above allows identifying graphically the 40 mV per unit of pH shift. Diamonds represent pH_i 5.5, squares pH_i 6.5 and triangles pH_i 7.5. *Figure taken from* [6].

Inhibition by polyvalent cations

Since voltage-gated proton channels were discovered, they have demonstrated to be inhibited by several cations as Zn^{2+}, Cd^{2+}, Cu^{2+}, Co^{2+} and La^{3+} [39]. Based on this and on different studies, DeCoursey describes the following relative potency for several polyvalent cations: $Zn^{2+} \approx Cu^{2+} \approx La^{3+} > Ni^{2+} > Cd^{2+} > Co^{2+} > Mn^{2+} > Ba^{2+}, Ca^{2+}, Mg^{2+} = 0$ [2].

Among all of them, inhibition by zinc is claimed to be the most potent one [95] and in fact, it was used initially for discriminating proton channels from potassium channels in *Helix aspersa* neurons because potassium channels are 80 times less sensitive to Zn^{2+} than H_V1 [1], [2].

Zinc inhibition is strongly regulated by pH_o being less sensitive at lower pH. For instance, lowering the external pH from pH 6 to pH 5 slows the channel' activation 100 times less and shifts the gH-V relationship 230-fold [96]. This behavior indicates that the channel present competitive inhibition for protonable binding sites accessible to the external solution, considering that the channel shows insensitivity when Zn^{2+} is applied by the internal solution [96].

In 2010, Musset *et al* tested the hypothesis that Zn^{2+} binding occurs in between the interface of the monomers conforming the dimeric hH_V1, specifically on two histidines residues: His140 and His193. This hypothesis was based on aspects as the exposition of both His residues to the external solution [3], the high possibility that responsible residues for a competitive inhibition by Zn^{2+} would have a pKa 6.-7 [96] and the complication to coordinate Zn^{2+} in a distance as the one separating both histidines into the same monomer [2]. In their experiment, Musset *et al* proved that in fact, Zn^{2+} binding happens in the dimer interface between pairs of His residues from the monomers, inhibiting the channel opening [54]. Moreover, the weaker effect of Zn^{2+} on monomeric channels is considered an evidence of the cooperative gating of the monomers, where the relative movement to each of them is an important step previous to opening [54].

Even though Zn^{2+} plays an important role in the channel inhibition, the effect is compromised to some extent to the presence of His residues. Thus, absence of both or one of them has an effect on the cation sensitivity, and in this way, is not the same for all species where H_V1 is present [2]. For example, *Ciona intestinallis* (1 His residue) has 27 times less sensitivity than mVSOP (2 His residues) and it is even less

in the cases of *Emiliana huxleyi* (no His residues) and *Karlodinium veneficum* (no His residues) [2].

1.5 Distribution across the species

The voltage-gated proton channel is widely distributed among species, from single-celled marine organisms to more complex ones, as humans [3] (**Figure 1.12**).

Single-celled organisms present higher sequence divergences in comparison with proton channels from higher organisms, where *Karlodinium veneficum* presents a major one. Less difference is found in invertebrates and even fewer in vertebrates. Mammals by their part show the closest homology among all the species. It is thought that sequence divergences are related with functional differences [63], for instance, *K.veneficum* has demonstrated to present proton inward currents [7] and considered the only proton channel with this characteristic, all the rest open only when there is an outward electrochemical proton gradient [63].

Presumed existence of H_V1 in algae, fungi and fewer higher plants has arrived according with recent BLAST searches [63]. In the case of higher plants and based on studies from Taylor *et al.* [97], it is thought that proton channels would be useless due to the fact that plants handle inward proton currents for driving nutrients absorption and solute exchanging that would provoke an electrochemical gradient adverse to H_V1 opening [6].

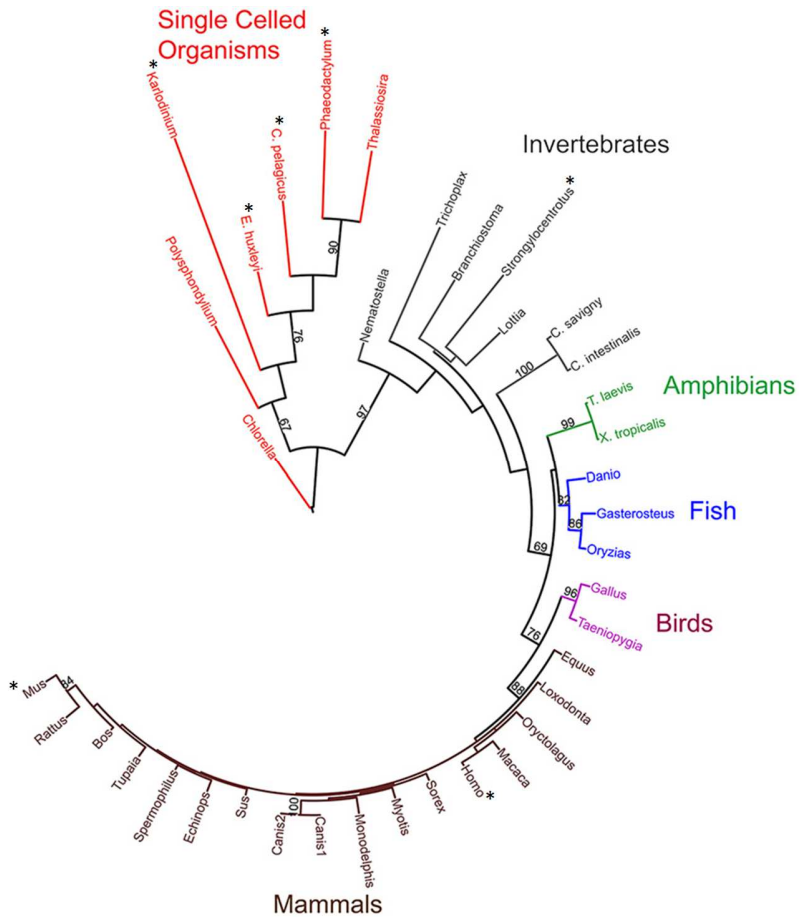

Figure 1.12. **Maximum likelihood phylogenetic tree based on the analysis of 37 H_V1.** The length of the branches is proportional to the difference in the sequence alignment. Species marked with an asterisk are those where the channel was confirmed by voltage clamp experiments. Another gen not shown has been identified recently in other bioluminescent dinoflagellate, *Lingulodinium polyedrum* [98]. *Figure taken from* [7].

Up to date, only one gen has been identified per species [63] [6]. In the sequence analysis done by Smith *et al.* [7], 37 species are candidates for having proton channels but among them, only eight has been confirmed by means of electrophysiological experiments (*Marked species from* **Figure 1.12**).

In general, the voltage-gated proton channel seems to be widely spread in living organisms, especially in the Animalia kingdom but never before found in the biggest class among it: the insects. However, in 2014 Misof *et al.* have published the most recent and complete genome data base for insects up to date [99] that has opened a window in the search for H_V1 candidates, where first tries have shown promising results.

2. Hypothesis

Examination of insect genomes based on Misof *et al.* work showed genes presenting high homology with H_V1, especially consistent in the case of the order *Zygentoma*.

One of the species among *Zygentoma*, *Nicoletia phytophila* (Nicoletiidae) has been hypothesized as candidate for the first identification of a H_V1 in insects.

For achieving the goal, the presumed new channel named NpH_V1, should be expressed heterologously in a system used in other studies. This would allow comparing the results with other voltage-gated proton channels.

3. Methodology

The putative H_V1 was heterologously expressed and later investigated by the patch-clamp technique. The RNA isolation, gene bank search and tissue expression were done by cooperation. These contributions and the methods applied are described in this section for more clarity.

Insect TSA data base was provided by 1KITE project.

N. phytophila animals were collected in Taman Rimba Templer, Selangor, Malaysia, in April 4, 2012. A total of thirty specimens were sampled, mashed and preserved.

The RNA was extracted from the whole insect body and transcribed into cDNA.

Both the animals' sampling and the RNA extraction were done by Yuta Mashimo and Ryuichiro Machida from the University of Tsukuba, Japan; meanwhile the RT-PCR

and the gene bank search were conducted by Christian Derst from the Universität zu Köln, Germany.

Mutants were produced by Arne Franzen from Forschungszentrum Jülich, Germany.

More details about contributions in this work can been seen in [64].

3.1 Gene identification

The channel identification was carried out by means of Basic Local Alignment Search Tool (BLAST) searching in the Transcriptome Shotgun Assembly (TSA) database for insects recently published by Misof *et al.* [99] as part of 1Kite project[1].

The identified sequences were later analyzed by using ClustalW for alignment [100] defining a R-x-W–R-x-x-R motif as determinant criteria. The selection of this criterion has been done considering that it is a well conserved part of the voltage-sensor motif located in the S4 segment of the channel.

3.2 Tissue expression of H_V1 in Zygentoma

From the BLAST analysis, consistent results of H_V1 homologues were found commonly in basal insects. Among them, the order Zygentoma presented the most successful results and therefore, was the insect's order selected for analyzing the channel's functional expression.

Due to its easy accessibility, the species *Thermobia domestica* commonly known as "firebrat", was chosen for the essays.

[1] http://www.1kite.org/

Six animals were manually dissected in order to extracting the mRNA from different tissues: nervous system (ganglia), leg muscle, body muscle and malpighian tubule.

An RNeasy Mini Kit (Qiagen, Hilden, Germany) was used for achieving mRNA isolation. Afterwards, cDNA was prepared by means of Sensiscript Reverse Transcriptase (Qiagen, Hilden, Germany).

Finally, a PCR was run using specific H_V1 primers derived from the GenBank TSA entry GASN011342010 (NCBI, 2014) (5´-GACCAGCAAACAATCGATCA-3´, 5´-TTTGACAGAACAAGACAGAATGC-3´) and Advantage Taq 2 polymerase mixture (Clontech). The PCR products were analyzed on an agarose gel and cloned into pGEM-T vector for sequencing.

3.3 DNA constructs

For the electrophysiological analysis, the full sequence of Zygentoma *Nicoletia phytophila* (NpH_V1) was chosen. This selection was done because of the partial retrieving for *Thermobia domestica* sequence and because of the close homology between the two species.

The NpH_V1 gene containing 5' BamH1 and 3' EcoR1 restriction sites was commercially synthetized by Eurofins/Genomics, Ebersberg, Germany.

The gene was cloned into the QBI-fC3 plasmid, which has been reported before for the human channel expression [49].

For distinguishing between transfected and not transfected cells, the Green Fluorescent Protein (eGFP) gene was fused to the N-terminus of the channel.

As well, NpH_V1 lacking of N-terminal eGFP was sub-cloned into pcDNA3.1 vector. This construct was used with the purpose of verifying if the physical attachment of eGFP changes the channel properties.

The mutants were obtained by site directed mutagenesis using a PCR overlapping procedure and their clones were confirmed by commercial sequentiation.

3.4 Secondary structure and phylogenetic tree

Two structure prediction programs were used for achieving the secondary structure of NpH_V1: STRAP [101] and WAGGAWAGGA [102].

An un-rooted phylogenetic tree of NpH_V1 and other six proton channels was done using PROTDIST (University of Washington, 2008).

3.5 Electrophysiological characterization

The electrophysiological analysis was carried out using the patch-clamp technique [103] with a set of instruments consisting in three kinds of components: optical, mechanical and electrical.

All the measurements were obtained with the same instruments, at 20 - 23 °C (room temperature). No leak correction was applied to any of the recordings.

3.5.1 Instrumentation

Optical components

The optical components consisted on a LEICA DMIL inversed optical microscope (Wetzlar, Germany) with a magnification power up to 400X and a ebq 100 mc-L U.V-discharge lamp (LEISTUNGSELEKTRONIK JENA, Jena, Germany).

Ultraviolet light was produced by a 35W·6V·G4 64275 low-voltage xenon bulb (OSRAM, Augsburg, Germany) operated by the discharge lamp.

Mechanical components

In general, the mechanical parts of the patch-clamp set comprised a Faraday cage, an anti-vibration table, a motorized manipulation unit, a headstage, a vacuum pump, solution exchange pipelines, an aluminum support column and a metal grounding block.

The assembly was done accordingly with the following description:

Both the aluminum column and the grounding block (house-made) were fixed to a MICRO-G four pointed pneumatic anti-vibration table (TMC, Massachusetts, U.S.A.).

A Faraday cage (house made) was situated over the table to prevent noise due to external electric fields meanwhile the measurements.

A Mini 25 three axes motorized manipulator unit (Luigs & Neumann, Raingen, Germany) was fixed to the aluminum column. To this one, a HEKA EPC-10 *usb* headstage was attached.

In order to control the pressure inside the pipette, a tube ending in a butterfly valve was connected to the lateral exit of the holder head.

The microscope was placed over the table just next to the manipulator arm.

The setup mechanical components can be seen in **Photography 3.1**.

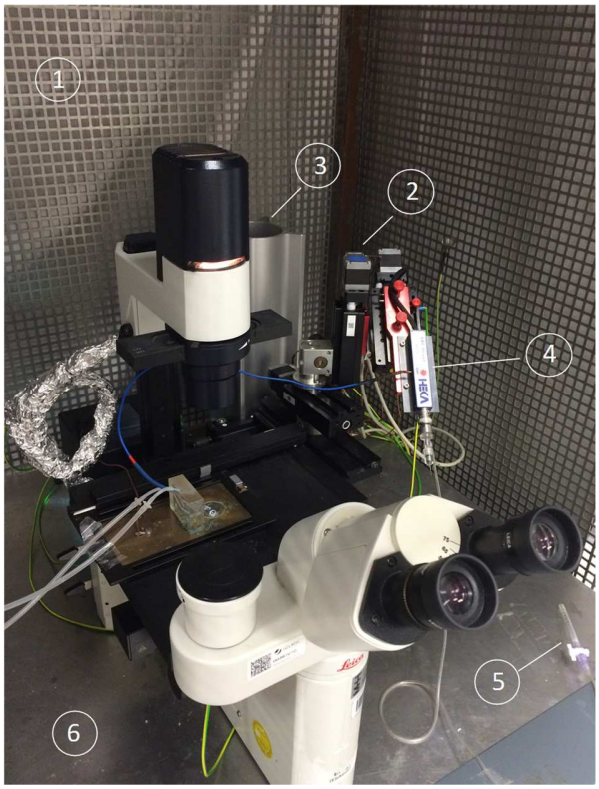

Photography 3.1. **Mechanical components.** 1) Faraday cage, 2) motorized manipulation unit, 3) aluminum support column, 4) headstage, 5) pressure control valve, 6) anti-vibration table.

All metallic components requiring on grounding were connected to the metal block fixed to the table. This joining block was at its time grounded by a connection to the Faraday cage.

Solutions' exchange during experiments was achieved by using a two tube system.

For exchanging to a desired solution, the solution was pumped-in with a syringe through the upper tube and the surface of the bath electrode.

Bath solutions were pumped-out through the lower tube using a VWR VP86 air vacuum pump (VWR International, Pennsylvania, U.S.A.). **Photography 3.2** shows the exchanging system described before.

The pump pipeline was connected to a filtering flask where all the residues were collected for final disposal.

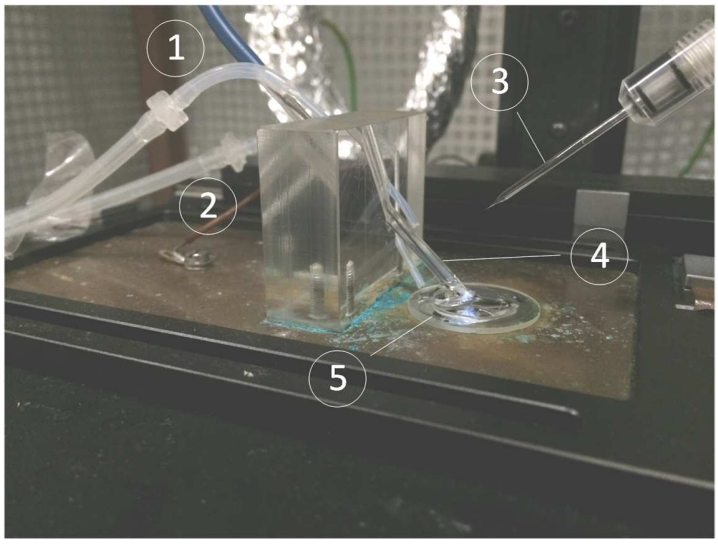

Photography 3.2. **Solution exchange system.** 1) Incoming solution tube, 2) outgoing solution tube, 3) pipette, 4) bath electrode, 5) bath chamber.

Electrical components

An amplifier, a manipulator control system, a digital filter and a desktop PC were part of the electrical components.

The current signals were recorded by with a HEKA patch clamp EPC 10 USB single amplifier (**Figure 1, C**) controlled by a PATCHMASTER 2.65 software; both from HEKA Elektronik (Ludwigshafen, Germany).

The manipulator control system was composed of two parts: a SM6 remote control / keypad and a SM6 3 axes control box (**Figure 3.1, A and B**), both products from Luigs & Neumann (Raingen, Germany).

Figure 3.1. **Electrical hardware components.** A) Remote control / keypad, B) Control box, C) Amplifier. *Source: HEKA Elektronic, 2016 and Luigs & Neumann, 2016.*

The currents were filtered at 20 Hz passing the signals through a WARNER INSTRUMENTS CORP LFP-8 lowpass filter (Connecticut, U.S.A.).

Electrical contact with the pipette solution was achieved by using a chloride covered silver wire (**Photography 3.2, 3**) meanwhile the circuit was closed through a reference electrode connected to the bath solution. This bath electrode consisted of

a AgCl wire that was connected with a Ringer-made agar bridge to the bath (**Photography 3.2, 4**).

A general view from the patch-clamp set is shown in **Photography 3.3**.

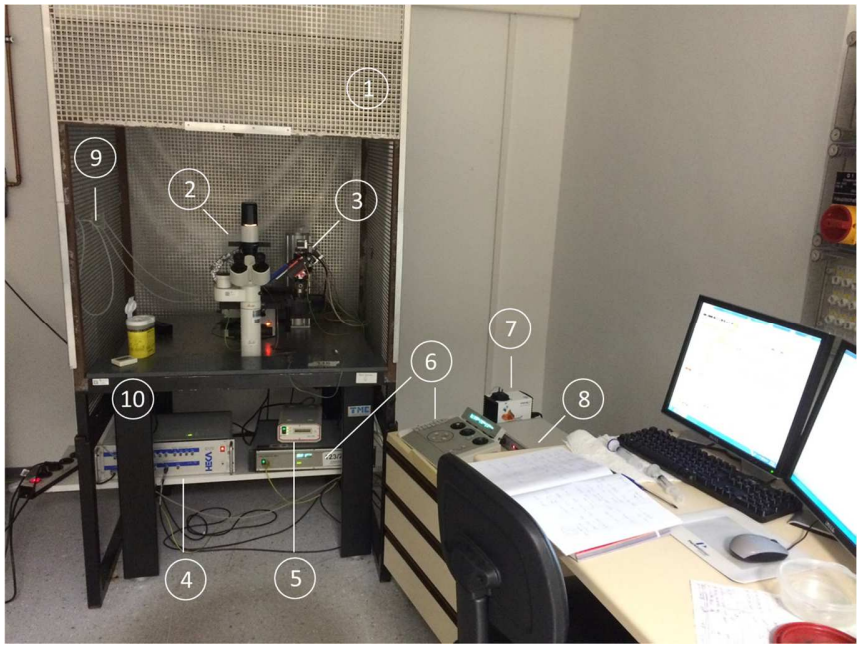

Photography 3.3. **Patch-clamp setup overview.** 1) Faraday cage, 2) microscope, 3) manipulator, 4) amplifier; 5) U.V lamp, 6) manipulator control system 7) pump 8) digital filter, 9) buffer exchange pipeline system, 10) isolation table.

3.5.2 Heterologous expression

tsA201 cells, derived from HEK cells, were used as expression system. The system selection was done considering its previous use in proton channel voltage-clamp studies as for instance in *Ciona intestinalis* [4], mouse [4], human [3] or dinoflagellates [7]; in order to obtain comparable results.

The cells were grown in 3.5 cm dishes at 85 % confluence, at 37 °C, in a 5 % CO_2 environment and using a commercial high glucose content media DMEM from Sigma-Aldrich.

Once the desired confluence was achieved, the cells were transfected with 1.3 μg of cDNA using polyethylenimine (PIE) from Sigma-Aldrich and incubated for 12 hours at 37 °C, 5 % CO_2. The transfection was confirmed by fluorescence under U.V. light after this time.

The cells were split using trypsin solution and re-plated on glass cover slips to generate isolated cells for patch-clamp recordings.

Patch clamp recordings were done the same or next day after cell's splicing. When the cells were patched the same day of splicing, a minimum waiting time of 3 hours between splicing and patching was maintained. This time frame is sufficient for the cells to adhere to the glass cover slips.

For testing if the physical attachment of eGFP changes or not the channel properties, co-transfections using NpH_V1-pcDNA3.1 (*see section 3.3*) and eGFP were done. In both cases a quantity of 1 μg of DNA were used. The rest of the transfection process was done as described before.

3.5.3 Micropipettes

Micropipettes were pulled using a Flaming Brown micropipette puller, Model P-1000 (Sutter Instruments, USA) from GC150F-10 borosilicate glass capillaries (1.5 mm OD x 0.86 mm ID x 100 mm L) (Harvard Apparatus, UK).

After pulling, the pipettes were polished by heat with a MICRO FORGE MF-830 (NARISHIGE, Japan) for getting a tip resistance between 5 – 10 MΩ with $TMA^+CH_3SO_3^-$ solutions. **Photography 3.4** shows the instruments used in this step.

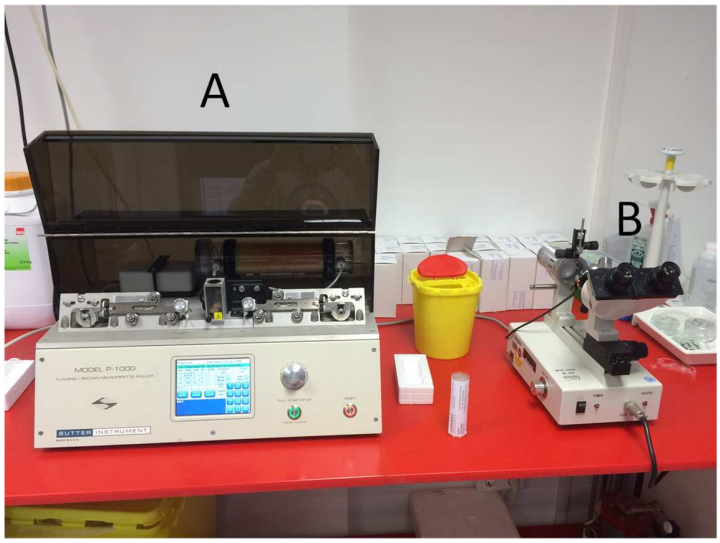

Photography 3.4. **Micropipette puller set.** A) Micropipette puller, B) Micro Forge

3.5.4 Working solutions

Pipette and bath solutions containing 20 - 190 mM buffer (pK_a close to working pH), tetramethylamonium (TMA^+) and methanesulfonate ($CH_3SO_3^-$) as main ions, 2 mM Mg^{2+} and 1 mM EGTA were prepared. The pH range for these solutions was from 4.5 to 8.0.

The detailed composition of each solution could be seen in **Table 3.1**.

Table 3.1. Solutions composition.

pH	Chemical (concentration in mM)								
	$MgCl_2$	EGTA	$TMA^+CH_3SO_3^-$	BIS-TRIS	HEPES	MES	Tricine	Homo-PIPES	BES
4.5	2	1	165	-	-	-	-	20	-
5.5	2	1	125	-	-	80	-	-	-
6.5	2	1	60	120	-	-	-	-	-
7.0	2	1	90	-	-	-	-	-	100
7.5	2	1	30	-	190	-	-	-	-
8.0	2	1	90	-	-	-	100	-	-

For all solutions, the osmolality was adjusted in the range of 290 – 310 mOsmol kg^{-1} and measured with a cryoscopic osmometer OSMOMAT 030 (GANOTEC, Berlin, Germany).

In ion selectivity essays, the methane sulfonate dominant ion was exchanged to chloride keeping the concentrations as described earlier, using tetramethylamonium chloride (TMACl) instead of $TMA^+CH_3SO_3^-$.

A $TMA^+CH_3SO_3^-$ 1 M stock solution was previously prepared by neutralization of tetramethylamonium hydroxide (TMAOH) with methanesulfonic acid (CH_3SO_3H).

The HEPES and MES buffers were supplied by SERVA (Heidelberg, Germany), the BIS-TRIS by AppliChem (Darmstadt, Germany) and the rest of reactants by Sigma-Aldrich.

The final pH for each solution was measured at 20 °C with a Knick 766 pH – Meter (Berlin, Germany).

All chemicals used and their specifications are shown in **Table 3.2**.

Table 3.2. **Chemical substances used.**

Reactant	Specifications	Supplier	pKa (25 °C)*
$MgCl_2$	Magnesium chloride	Sigma-Aldrich	
EGTA	Ethylenglycol tetraacetic acid	Sigma-Aldrich	
BIS-TRIS	Bis(2-hydroxyethyl)amino-tris(hydroxymethyl)methane	AppliChem	6.50
HEPES	4-(2-hydroxyethyl)-pipperazine-1-ethanesulfonic acid	SERVA	7.48
MES	4-Morpholineethanesulfonic acid	SERVA	6.10
Tricine	N-[Tris(hydroxymethyl)methyl]glycine	Sigma-Aldrich	8.05
Homo-PIPES	Hexahydro-1H-1,4-diazepine-1,4-bis(2-ethanesulfonic acid)	Sigma-Aldrich	4.55
BES	N,N-bis[2-hydroxyethyl]-2-aminoethanesulfonic acid	Sigma-Aldrich	7.09
TMAOH	Tetramethyl ammonium hydroxyde	Sigma-Aldrich	
CH_3SO_3H	Methane sulfonic acid	Sigma-Aldrich	
TMACl	Tetramethyl ammonium chloride	Sigma-Aldrich	
DMEM	Dulbecco's Modified Eagle's Media 1X. 1000 mg/L glucose, sodium bicarbonate, pirydoxine.	Sigma-Aldrich	
PEI	Polyethylenimine. branched. $H(NHCH_2CH_2)nNH_2$	Sigma-Aldrich	

**when applies.*

3.5.5 Recordings

Glass cover slips containing transfected tsA201 cells were placed into a polyacrilate chamber (**Photography 3.2, 5**) and covered with bath solution.

To avoid interferences due to either bacterial or any other material in the solutions, both the pipette and the bath solutions were filtered previously to their use. Filtrations were done by means of disposable syringe filters with a pore size of 0.20 μm (Sartorious, Göttingen, Germany).

The transfected cells were detected with the microscope by distinct staining of the membrane under the fluorescent light.

Fluorescent cells were later tight-sealed to pipettes with help of the micro-manipulator and patch-clamped using a "Whole - cell" configuration.

Cell sealing and opening

Pipettes were filled up with the desired solution and placed in the headstage. In order to keep the pipette without contamination, a smoothly positive pressure was applied through the lateral valve of the headstage. This small pressure is sufficient for creating an outward flux of the pipette solution and therefore avoiding the obstruction of the tip.

The current was zeroed when pipettes and bath solution entered in contact, and once the pipette was over the cell membrane just before touching it.

Contact between the pipette and the cell surface was determined by an increase of the pipette resistance.

When the cell contact was achieved, seals were formed by applying a gentle negative pressure throw the pipette until the resistance achieved ≥ 1 GΩ (gigaseal). During the process, the holding potential was set at 0 mV.

In cases where the gigaseal could not be reached, the cell membrane was polarized by setting the holding potential (V_{hold}) at –40 mV once a minimum resistance of 200 MΩ was reached. In some cases, sealing was obtained after some waiting time.

After sealing, the fast capacity transients associated with the pipette capacitance to the bath solution were compensated.

The access to the interior of the cell was done by applying a smoothly suction through the pipette, confirmed by the appearance of large capacity transients.

After compensating the large capacity transients, the holding potential was settled according with the desired working protocols.

Test pulse protocols

Test pulse protocols were applied in 10 mV increments from voltages close to the holding potential up to potentials were depletion of protons was evident.

The holding potential for each of the measurements was chosen considering the Nernst potential for protons (E_H) under the working conditions, in order to ensure well defined tail currents.

V_{rev} determination protocols

In order to determine the V_{rev}, two different strategies were applied:

If the voltage threshold of activation (V_{thres}) was positive to V_{rev}, the traditional tail current method [94] was applied. In this procedure, the holding potential was set in a value more negative than the V_{rev}, a pre-pulse was applied in order to obtain significant proton outward currents. After this pre-pulse, the membrane potential

(E_m) was set at the testing potential in increments of 10 mV per sweep. A general representation of a tail current protocol could be seen in **Figure 3.2**.

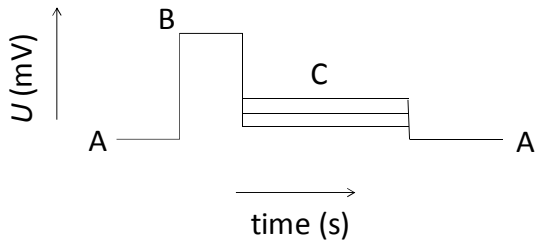

Figure 3.2. **Traditional tail current protocol diagram.** A) Holding potential, B) pre-pulse, C) test pulse.

Considering that the applied pre-pulse could change the zero potential by a few millivolts due to depletion of protons [104], different pre-pulse voltages were tested in every determination in order to reduce this source of error.

Finally, in cases where V_{rev} was positive to V_{thres}, it was determined by interpolation between time-dependent inward and outward currents during test pulses.

3.5.6. Data analysis

The data analysis was carried out by means of the FITMASTER 2.65 software from HEKA Elektronik and by OriginPro 7 from OriginLab Corporation (Northamptom, MA, USA).

Threshold potential: V_{thres}

The V_{thres} was determined from the pulse protocols as the first appearance of either and outward or inward proton current. To avoid confusion with pipette capacitance components, the plausible proton current was only taken as real when an evident tail current appeared after the depolarizing pulse.

Maximal proton current: $I_{H,max}$

The maximal proton current was obtained by single exponential function fitting of the activation component (**Equation 3.1**). A short delay was considered in every fitting and the maximal extrapolated value was then taken as the $I_{H,max}$ for the corresponding pulse (*see* **Figure 3.3**).

$$y = y_0 + Ae^{\frac{x}{\tau}}$$

(Equation 3.1)

where:

y_0 *= offset.*

A *= amplitude.*

τ *= time constant.*

Activation kinetics: τ_{act}

Activation kinetics were determined as the time constant (τ) obtained from the single exponential fitting (**Equation 3.1**). This time component was calculated for each sweep of the activation phase.

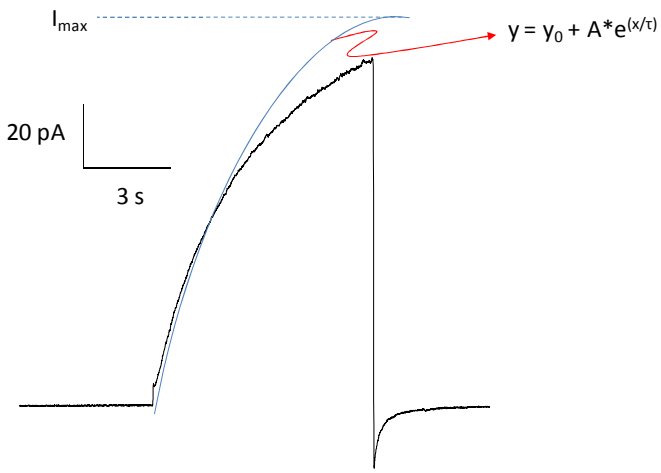

Figure 3.3. **Activation component fitted to a single exponential function.** The blue curve represents the data fitting, where A = I_{max}, y_0 is the offset and τ is the 63.2 % of the maximal response.

Maximal conductance for protons: $g_{H,\,max}$

The maximal conductance for protons was calculated as the quotient between the maximal current and the corresponding voltage pulse, and considering the leak current (I_{leak}) as following:

$$g_{H,max} = \frac{(I_{max} - I_{leak}) - I_{rev}}{V_{test} - V_{rev}}$$

(Equation 3.2)

where:

$g_{H,max}$ *= maximal proton conductance.*

I_{max} *= maximal proton current.*

I_{leak} *= leak current.*

I_{rev} *= current at reversal potential.*

V_{test} *= test pulse potential.*

V_{rev} *= reversal potential.*

Equilibrium potential: V_{rev}

The reversal potential or equilibrium potential was estimated directly from the tail current protocol signals, determined as the flat line in between the inward and outward currents from the time dependent components. The same logic has been applied for events where V_{rev} was positive to V_{thres}.

In cases where running a tail current protocol was not possible, V_{rev} was calculated by the X axis interception (zero current) of a line connecting the end pulse current (I_{end}) with the tail current (I_{tail}) for the corresponding pulses (V_{test} and V_{hold}). This procedure has been applied and validated before by Musset *et al.* [70] (*see* **Figure 3.4**).

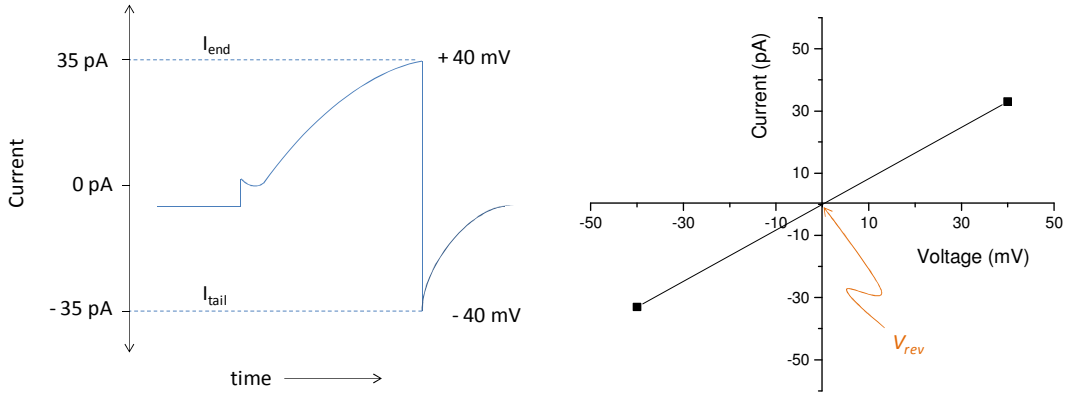

Figure 3.4. **X axis interception method for V_{rev} estimation.** Hypothetical situation with a resulting V_{rev} = 0 mV, where I_{end} = + 35 pA measured at the end of a + 40 mV pulse and I_{tail} = -35 pA corresponding to a holding potential of – 40 mV.

Liquid junction potential

The liquid junction potential (LJP) was determined experimentally as described by Barry P.H [91] and Neher [105].

4. Results

4.1 Channel identification

Based on the BLAST, several insects present DNA sequences closely related to other known voltage-gated proton channels. The candidates showed homology with the conserved motif of the putative voltage-sensor domain, R-x-WR-x-x-R, located in the fourth transmembrane domain (S4) of the protein. This pattern has been described before in other species [3], [4], [106], [7], [97].

Among the insect genomes analyzed so far, basal insects, a more primitive group among them, displayed consistently presence of H_V1 homologues. Hence, DNA homolog sequences were detected in the order Zygentoma, Archeognatha, Protura and Diplura. However, no H_V1 homologues were found in the closely related Collembola.

In the case of higher insects, possible candidates could be found exclusively in some polyneopterans. Single findings in Hemiptera and Diptera showed putative H_V1 homologues but these are single findings which could not be found in other species from the same orders. In addition, the cDNA from these single findings present high homology with fungus DNA, therefore it is likely that single findings in Hemiptera and Diptera are artifacts.

A list of the species where putative H_V1 homologues were detected could be seen in **Table 4.1**.

Table 4.1. **Insect species with putative proton channel homologues.**

Order	Species
Diplura (two-pronged bristletails)*	*Occasjapyx japonicus*
	Catajapyx aquilonaris
Protura (coneheads)*	*Nipponentomon nippon*
	Acerentomon sp.
	Filientomon takanawanum
Archaeognatha (jumping bristletails)*	*Pedetontus okajimae*
	Machilis hrabei
	Machilontus sp.
Zygentoma *	Tricholepidion gertschi
	Thermobia domestica
	Atelura formicaria
	Nicoletia phytophila
Dermaptera (earwigs)	*Forticula auricularia*
Orthoptera (crickets and katydids)	*Ceuthophilus sp.*
Embioptera (webspinners)	*Aposthonia japonica*
Mantodea (praying mantids)	*Metallyticus splendidus*
Phasmatodea (stick and leaf insects)	*Extatosoma tiaratum*
	Sipyloidea sipylus
	Ramulus artemis
	Medauroidea extradentata
Hemiptera (bugs, cicadas, plant lice)	*Acanthocasuarina muellerinae*
Diptera (true flies)	*Bactrocera minax*

** Basal insects*

4.2. *Nicoletia phytophila* proton channel: topology and identity with other H_V1

Following common nomenclature used in proton channels, the protein has been named NpH_V1, where "Np" is the abbreviation for the species *Nicoletia phytophila*,

"H" is for the conducting ion (H^+), "*V*" subscript does reference to channel gating controlled by voltage and "1" refers to the first isoform found.

NpH_V1 consist in a protein of 239 amino acids with structural characteristics known for proton channels. Thereby, accordingly with the structural prediction methods used, the protein is formed by four transmembrane alpha helices: S1, S2, S3 and S4. The lacking of two transmembrane domains S5 and S6 in NpH_V1 is one of the features of all the H_V1 and a difference with other ion channels. In addition, NpH_V1 shows both the N-terminus and the C-terminus as being cytoplasmatic domains.

Figure 4.1 shows a cartoon of NpH_V1 amino acids sequence and some topological characteristics.

In comparison to other proton channels, NpH_V1 has the same highly conserved sequences: an aspartate residue in the middle of S1 (Asp66), three argenine residues in the S4 (Arg157, Arg160 and Arg163) and a tryptophan just over the second argenine in S4 (Trp159). These sequences are important for the function of H_V1 and are present in all the voltage-gated proton channels known so far.

An aspartate in the middle of S1 is the selectivity filter of H_V1 [49] [7] [73], and positive residues in the S4 of voltage-sensing domains (VSD) in other voltage-gated channels are responsible of voltage sensing during depolarization [67] [51]. In the case of H_V1, a pattern of positive charges (three arginines in S4) separated by two hydrophobic residues is found consistently among all orthologs [62]. Furthermore, the highly preserved tryptophan next to the second arginine in S4 has been considered essential for the biophysical behavior of the channel [84].

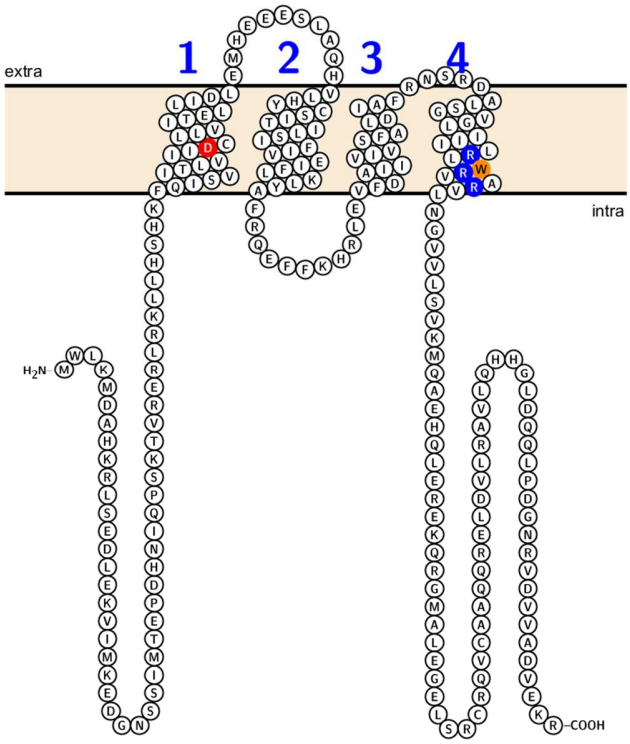

Figure 4.1. **Representative cartoon of *Nicoletia phytophila* voltage-gated proton channel.** Numbers from 1 to 4 represent the corresponding transmembrane domains (S1, S2, S3 and S4). In red: Asp66; In blue: Arg157, Arg160 and Arg163; In green: Trp159. *Visualization generated by PROTER* [107].

The alignment of NpH_V1 with other H_V1 is depicted in **Figure 4.2.** Here the alignment shows conserved patterns in NpH_V1 and other species.

It has been reported that the C-terminus consist in a coiled-coil which allows the channel to exist as a dimer [47] [45].[55].

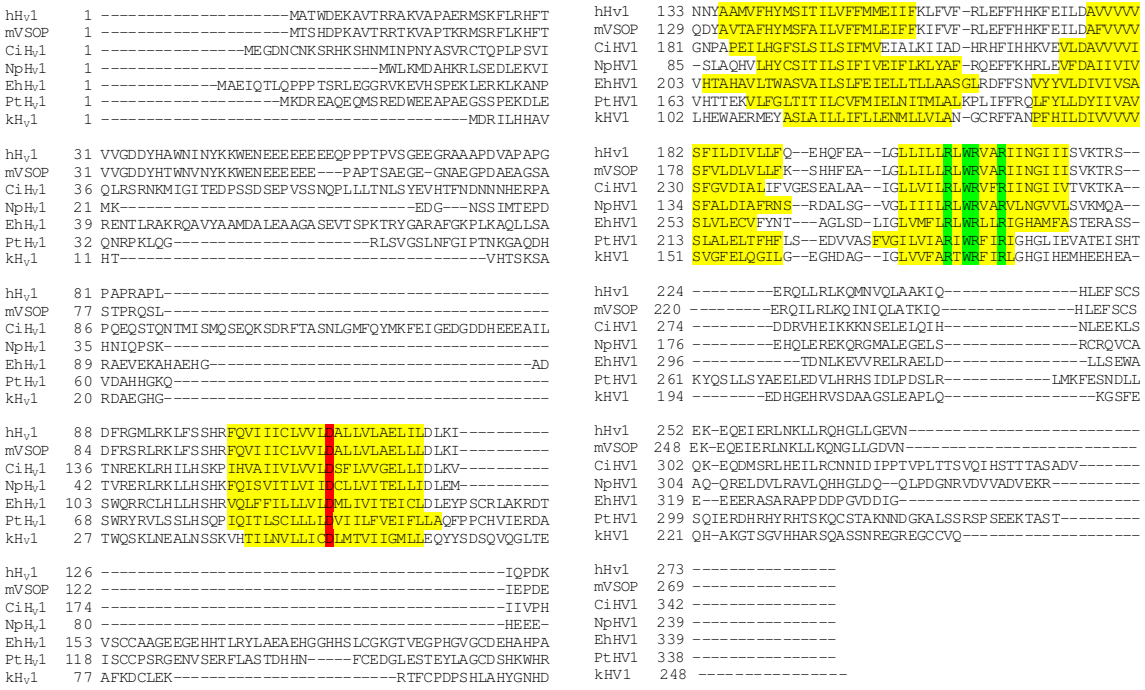

Figure 4.2. **Clustal W (1.8) multiple sequence alignment of different H_V1.** Yellow regions represent the presumed transmembrane segments S1-S4. Colored in red an Asp in the S1, the putative selectivity filter, and in green the characteristic pattern RxWRxxR present in all H_V1. hH_V1 = human, mVSOP = mouse, CiH_V1 = *Ciona intestinalis*, NpH_V1 = *Nicoletia phytophila*, EhH_V1 = *Emiliana huxleyi*, PtH_V1 = *Phaeodactylum tricornutum,* kH_V1 = *Karlodinium veneficum*.

In the case of NpH_V1, prediction of the coiled-coil motif was not possible due to contradictory results obtained with the different prediction programs. In this way, a coiled-coil C-terminus was predicted by WAGGAWAGGA but not by STRAP. This made it impossible to ensure that NpH_V1 is a dimer like most H_V1 or a monomer like kH_V1 [7] or PtH_V1 [97].

For a simple representation, a structural model of NpH_V1 (**Figure 4.3**) has been done by means of the SWISS-MODEL server [108]. After the automated alignment procedure, the crystal structure of the chimeric protein mH_V1cc, the only proton channel crystallized until now [50], has been chosen as a template. The NpH_V1

model and the crystal structure template share a sequence identity of 41 %. A further visualization was done by UCSF Chimera [109].

In this NpH_V1 close - state model, the lacking of N-terminus and the existence of a coiled-coil in the C-terminus are a consequence of the template used. In the mH_V1cc structure, the authors have reported the replacement of the C-terminal coiled-coil with a leucine-zipper domain from *S. cerevisiae* and the truncation of 74 residues forming the N-terminal [50].

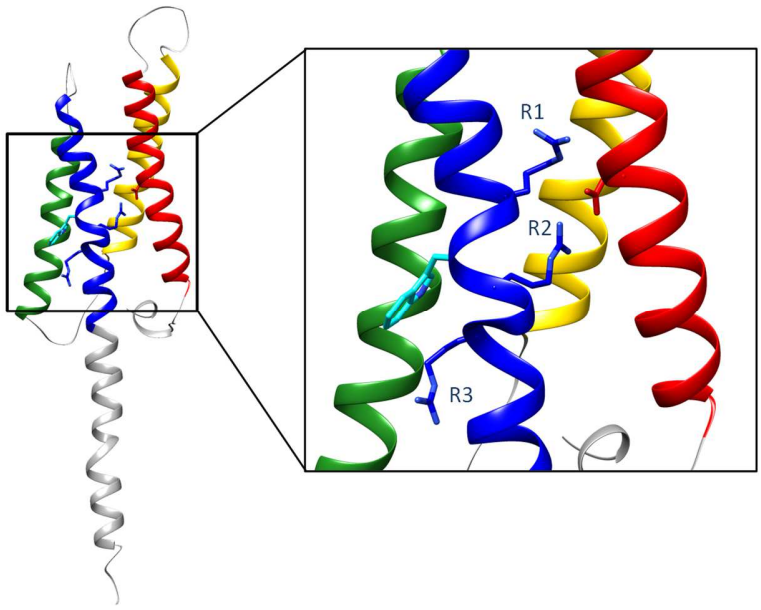

Figure 4.3. **Structural model of NpH_V1 in the closed state.** Ribbon traces of the four α-helical transmembrane domains are represented by different colors: in red, S1; in yellow, S2; in green, S3 and in blue, S4. The magnified region shows the location of clue residues: in blue the three arginines in S4, in cyan the tryptophan just over the second arginine of S4 and in red the aspartate in the middle of S1.

4.3 Heterologous expression of NpH_V1

tsA201 cells have been used in many patch clamp studies to evaluate the functionality of ion channels [110] [111] [112] [110] [113]. They consist in a human embryonic kidney cell line which has been transformed from HEK293 cells with the SV40 virus, reporting a widely use in functional expression assays[2].

The basis of the high expression levels reached with tsA201 seems to be related with amplification of the expression vector in the cytosol and/or cell´s relatively high transfection efficiency [114].

In the case of the voltage-gated proton channel, this expression system has been used in studies related with function and structure of the protein with satisfactory results [3], [4], [7], [115].

Using the proposed methodology, it was possible to achieve a good expression of NpH_V1 in mammalian cells. As it can be seen in **Photography 4.1**, the expression level reached with this method leads to transfection levels estimated in approximately 25 % of the cells according to visual counting. In addition, the fluorescence intensity emitted by the eGFP was strong enough to allow an easy single cell selection.

Incorporation of NpH_V1 plasmid with PEI vector is possible due to the DNA-PEI complex formation. The union forms a positive charged complex that can bind to the negative surface of the cells, facilitating its incorporation via endocytosis. [116]–[118].

[2] http://www.sigmaaldrich.com/catalog/product/sigma/96121229?lang=de&region=DE

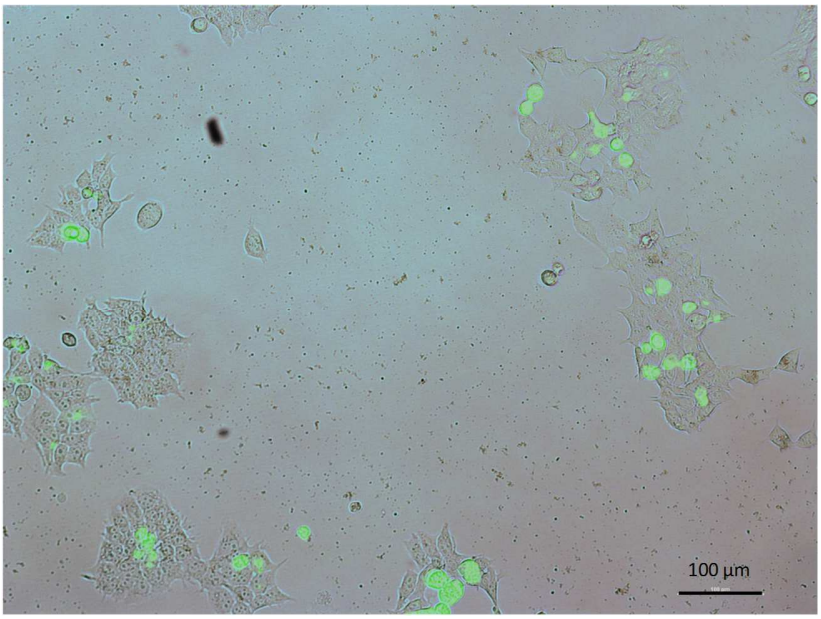

Photography 4.1. **tsA201 cell culture transfected with NpH_V1-eGFP**. Transfected cells show fluorescence due to excitation of the GFP with ultraviolet light, demonstrating successful expression of NpH_V1.

Figure 4.4 shows a comparison between currents obtained from patch clamped tsA201 control cells and transfected cells. Comparing to controls, clear current differences can be seen in those cells which have been over expressed with the channel. In the case of the transfected cell, its current density is approximately 13 pA / pF at + 30 mV and its V_{thres} determined in 0 mV (**Figure 4.4 B**). On the other hand, the tsA control cell presents dubious signals that in case of being proton currents, would have a current density of 0.5 pA / pF at + 110 mV and a presumed V_{thres} of + 70 mV (**Figure 4.4 A).**

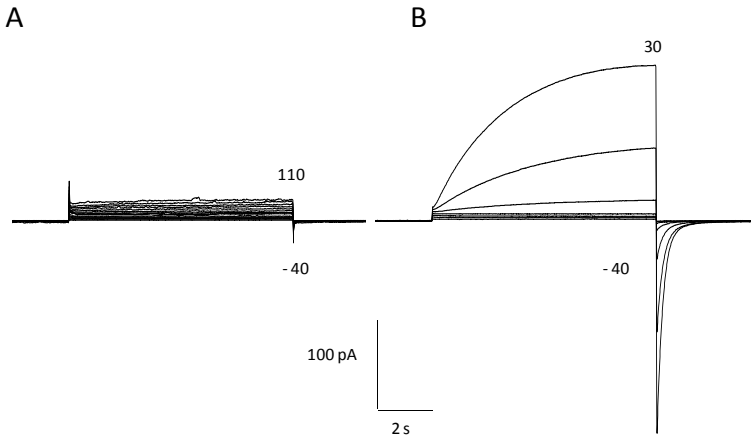

Figure 4.4. **Comparison between a tsA201 control cell and the same cell line transfected with NpH_V1.** Whole-cell family of pulses for two cells obtained with 10 mV increments from a holding potential of – 40 mV up to the value shown. Both cells measured at pH_i = 6.5, pH_o 6.5. A) a 11.2 pF tsA control cell. B) a 13.02 pF tsA cell transfected with NpH_V1 WT.

Differences on the V_{thres} between expressed and native proton channels have been previously demonstrated [70] and because of this, comparing values at the same voltage pulse may lead to a wrong result. A quick way to establish a reliable comparison between the currents amplitude during an experiment would be choosing the same voltage range over the V_{thres}. For example, a range of 30 mV over the V_{thres} could be defined as parameter. However, despite of being an easy and fast method, it doesn´t take in count the driving force. Moreover, the selection of the voltage magnitude over the V_{thres} must be done carefully. High cell depolarization would cause proton depletion and therefore, underestimated proton currents. In addition, cells' capacitance must be similar.

In the example from **Figure 4.4**, comparative I_{end} values can be taken at + 30 mV and + 100 mV for the transfected and not transfected cell, respectively. Hence and as it can be seen in a glance, the difference between both is considerable, showing values

of 172 pA for the transfected cell and 5.2 pA for the non-transfected; even though the driving force in the second case is much bigger.

Other way to establish a reliable comparison is doing it directly with the maximal conductance for protons. Here, the results show again a big discrepancy between control cells and the transfect ones. In the case of the first ones, the $g_{H,\,max}$ value is 0.2 nS, a conductance 30-fold smaller than 6 nS from the transfected cells.

Moreover, the V_{thres} detected in the control cells was about + 70 mV. This defers completely from values reported for native channels [5], [70], which could indicate that the recorded currents do not correspond to H^+ currents.

Both together, the fluorescence detection and the magnitude of the currents, indicate a successful heterologous expression of NpH_V1 in tsA201 cells. Here the over expression of the channel is clear.

4.4 NpH_V1 shows proton conduction and voltage-dependent gating

The voltage-gated proton channel presents several biophysical characteristics that make it different to other ion channels. Among them and how its name resembles, the channel gating is dependent of an electrical potential across the membrane: "it opens and conduct proton currents upon depolarization of the membrane" [5].

Figure 4.5, A, despites a classical voltage-clamp measurement for NpH_V1. Here it is possible to see consistent voltage-dependent outward currents when depolarizing pulses were applied at different pH_o // pH_i conditions.

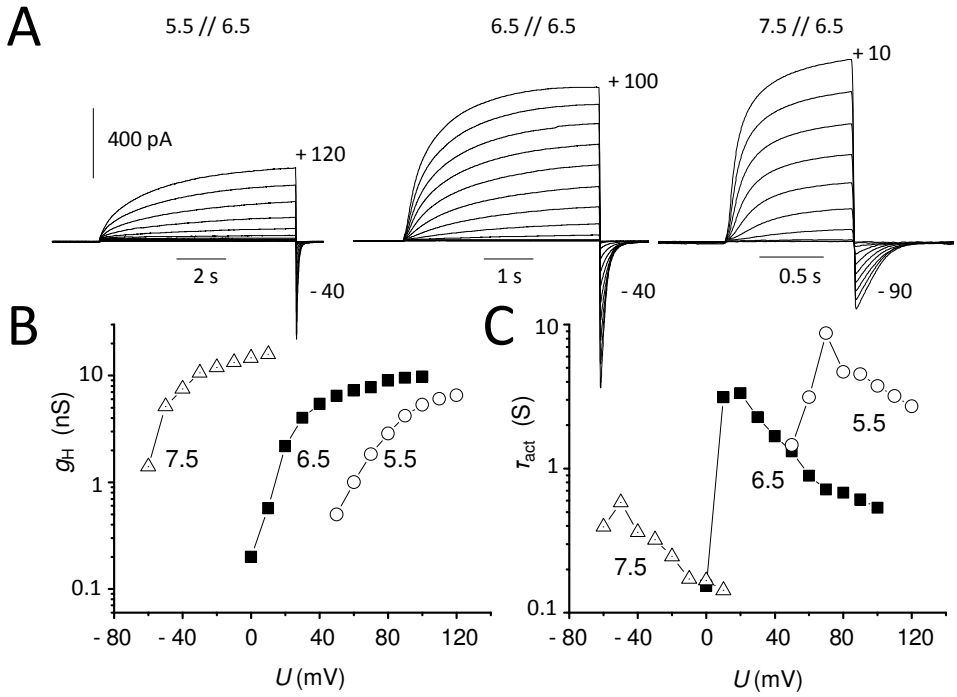

Figure 4.5. **NpH_V1 characteristic measurement.** A) Typical whole-cell measurement at different pH, indicated as pH_o // pH_i. The holding potential was -40 mV at pH_o = 5.5 and pH_o = 6.5, and – 90 mV at pH_o = 7.5. Family of pulses obtained with increments of 10 mV up to the voltage shown. B) Conductance – voltage plot at pH_i 6.5 and different pH_o (values shown). C) Activation kinetics.

Transfected cells with WT NpH_V1 showed maximal conductance around 10 – 20 nS with an average capacity of 8.3 ± 4.3 pF (n = 32 cells).

It has been proposed before that untransfected tsA201 cells don´t show clear outward or inward current [4], and because HEK293 cells reported a small background of ~ 1 pA/pF at + 150 mV and pH_i = 6.5 [26], measured currents are another indicative of good expression of NpH_V1 in a mammal cell line.

Currents showed monotonic voltage dependence, there was no saturation of the currents during strong depolarization, increasing with every positive pulse applied.

This characteristic has been described before as an important difference between H_V1 and carriers [5].

Moreover, no currents were detected before reaching certain membrane potential, V_{thres}, a conclusive proof of voltage dependent of gating. At symmetrical pH conditions, the average V_{thres} was estimated in 3.1 ± 8.4 mV (n = 28 cells).

As well, currents presented slow activation kinetics during depolarization, in the order of seconds, getting faster when the membrane potential became more positive (**Figure 4.5 A and C**). This slow activation behavior has been proposed as one of the special features from proton channels [1], [3], [4], [93].

In addition, presence of inward tail currents during repolarization were detected when the proton gradient was inward (**Figure 4.5 A, left**). This behavior was described by Sasaki *et al*. when the discovery of H_V1 and claimed to be indicative that currents belong to a channel and not to a pump [4].

Accordingly with the results, the gating showed not only voltage dependence but was strongly affected by the pH across the membrane as well, a unique hallmark for proton channels. This pH effect on gating can be seen either directly in the family of pulses (**Figure 4.5 A**) or as a shift on the conductance – voltage relationship (**Figure 4.5 B**).

Apparent current droops during measurements were attributed to proton depletion of the cytosolic protonated buffer. During large depolarizations, proton depletion is an important phenomena to take in count when measuring H_V1 [1], [104], [119], [120], where a complete buffer replenishment can take several minutes [121]. The result is an increase of pH_i that shifts E_H positively, reducing the driving force (V_m – E_H).

Figure 4.6 exposes an example of depolarization time reduction applied to avoid current underestimation due to proton depletion.

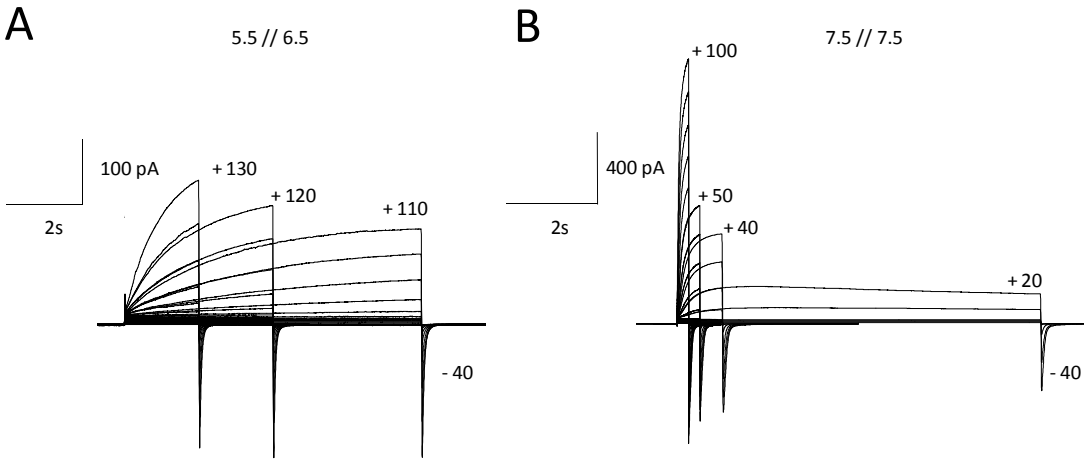

Figure 4.6. **Depletion of protons during whole-cell measurements.** Families of depolarizing pulses for two different cells, A and B, transfected with NpH_V1 WT. Pulses were applied from – 40 mV until the indicated voltage, in 10 mV increments. pH conditions are showed as pH_o // pH_i.

In order to determine if the physical attachment of GFP to NpH_V1 in the N-terminus affects the behavior of the channel, co-transfections of eGFP and NpH_V1 without the attached fluorescent protein were done.

The results didn´t show any significant difference in comparison with the measurements done for NpH_V1 – GFP, neither in the voltage dependence of gating, nor in the channel conductance or in the activation kinetics (**Figure 4.7**). The physical attachment of eGFP in the N – terminus, doesn´t affects the biophysical properties of the channel in a recognizable manner.

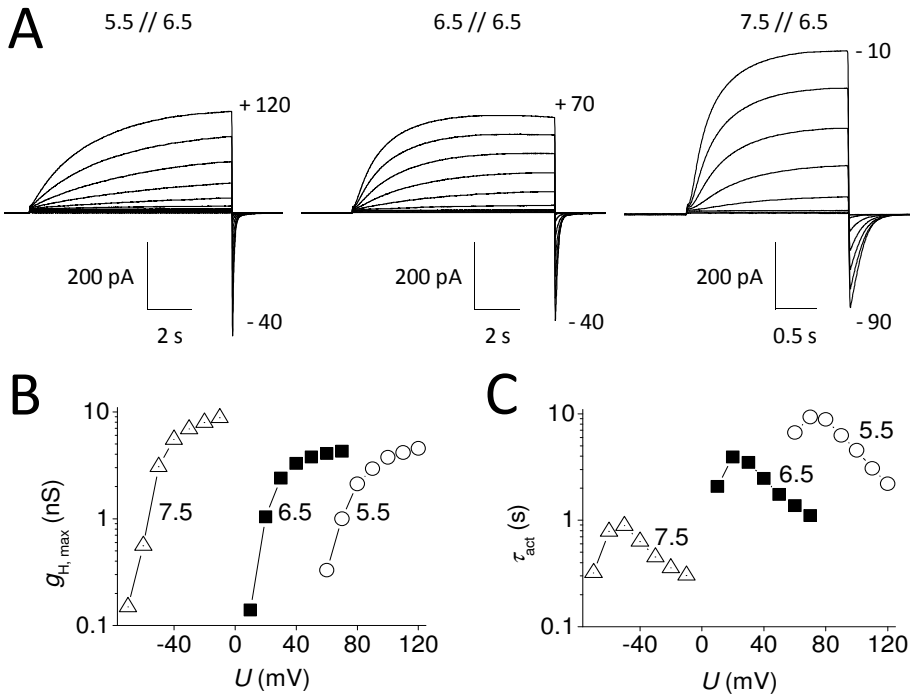

Figure 4.7. **NpH_V1 no GFP doesn´t show differences to NpH_V1-GFP.** A) Typical whole-cell measurement at different pH, indicated as pH_o // pH_i. The holding potential was -40 mV at pH_o = 5.5 and pH_o = 6.5, and – 90 mV at pH_o = 7.5. Family of pulses obtained with increments of 10 mV up to the voltage shown. B) Conductance – voltage plot at pH_i 6.5 and different pH_o (values shown). C) Activation kinetics.

4.5 Is NpH_V1 a proton channel?

Among others, the features described before: well defined voltage and pH dependence of gating, slow outward currents during depolarization, monotonic voltage dependence and presence of inward current during repolarization at inward proton gradients; made NpH_V1 a qualified proton channel suspect.

However, maybe the most important characteristic for proton channels is their perfect selectivity and therefore, should be tested in order to define it as one.

A way to evaluate the proton selectivity is by means of relative permeability described by the GHK equation (**Equation 1.1**). Hence, in presence of a proton selective channel, proton currents should reverse close to the Nernst potential for protons, E_H.

Figure 4.8 summarize the results of measured V_{rev} for 32 cells transfected with WT NpH_V1. In order to compare with E_H, a dotted line representing equality of both values is shown.

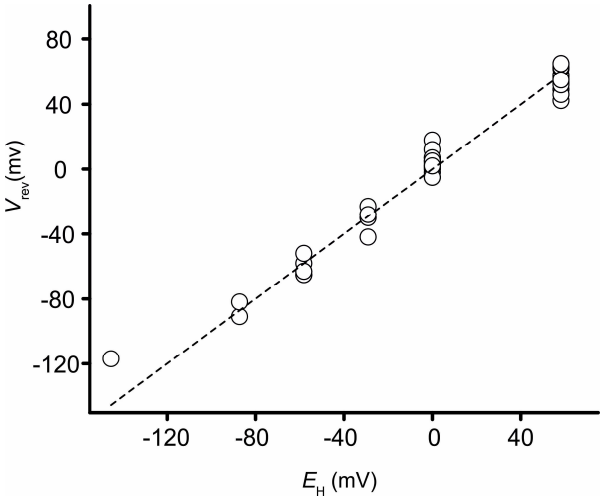

Figure 4.8. **Measured reversal potentials.** The V_{rev} measured for each cell is plotted against the Nernst potential for protons E_H. Measurements taken over a wide pH range: pHi (5.5, 6.5, 7.5) and pHo (4.5 to 8.0). The dotted line represents $V_{rev} = E_H$. n = 32 cells.

As it can be concluded, all the data follows the Nernst potential for protons along a wide range of pH_i (4.5 – 8) and pH_o (5.5 – 7.5); indicating high proton selectivity.

Accordingly with the buffer composition, GHK equation acquires the form:

$$V_{rev} = \frac{RT}{zF} \ln \left(\frac{P_{TMA^+}[TMA^+]_o + P_{Cl^-}[Cl^-]_i + P_{CH_3SO_3^-}[CH_3SO_3^-]_i + P_{OH^-}[OH^-]_i + P_{H^+}[H^+]_o}{P_{TMA^+}[TMA^+]_i + P_{Cl^-}[Cl^-]_o + P_{CH_3SO_3^-}[CH_3SO_3^-]_o + P_{OH^-}[OH^-]_o + P_{H^+}[H^+]_i} \right)$$

(Equation 4.1)

When permeability of all ions except H^+ is precluded, **Equation 4.1** becomes:

$$V_{rev} = \frac{RT}{zF} \ln \left(\frac{P_{H^+}[H^+]_o}{P_{H^+}[H^+]_i} \right)$$

(Equation 4.2)

This equation has the same expression than the Nernst equation, E_H (**Equation 1.2**).

Generating a pH gradient across the membrane will then shift V_{rev} in approximately 58 mV at 20 °C, according to E_H. The same shifts were obtained when pH_o was changed in one unit below or above pH_i (**Figure 4.8**)

Small deviations of V_{rev} respect to the predicted E_H are thought to be a consequence of deficient control of pH during the measurements, a common experimental error when measuring proton channels [5].

Doing a quick calculation based on the composition of the working solutions (*see* **Table 3.1**), proton concentration was 5.5 x 10^3 and 1.0 x 10^6 fold smaller than $CH_3SO_3^-$ or TMA^+ concentration at pH 4.5 and pH 7.5, respectively. Therefore, proton selectivity should be at least higher than those values taking in count that permeation of either $CH_3SO_3^-$ or TMA^+ would deviate V_{rev} from E_H (**Equation 4.1**).

The high selectivity detected is in accordance with the one proposed for proton channels, established as minimum 10^6 times higher than K^+ or Na^+ under physiological conditions [2]. In fact, previous works have demonstrated that no other ion permeates through H_V1; no other perfectly selective voltage-gated ion channel is known [6].

4.6 pH-dependence of gating

As it was discussed, proton currents in NpH_V1 showed a clear voltage dependence of gating but regulated by both pH_o and pH_i. In this sense, activation of g_H was shifted to more positively or negatively voltages, depending on the pH gradient applied (**Figure 4.5 B**)

In order to analyze the pH dependence of gating, V_{thres} for 32 cells was plotted against their V_{rev} (**Figure 4.9**) This method developed by DeCoursey and Cherny [90] has been commonly used in proton channel studies [4], [13], [29], [48], where the following linear correlation is obtained:

$$V_{thres} = slope\ x\ V_{rev} + offset$$

(Equation 4.3)

The slope obtained gives information about the pH dependence of gating, where higher values indicate higher gating variations when the pH across the membrane is altered. In a contrary situation, lower slopes represent fewer pH-dependent gating.

On the other hand, the offset value allows knowing the direction of the net proton flux along a pH range. Because in a linear regression the offset is the ordinate interception when the abscissa value is equal to 0, at symmetrical pH conditions

(V_{rev} = 0), a negative offset indicates the possibility of observing inward currents; meanwhile positive offsets are retrieved when outward currents are present.

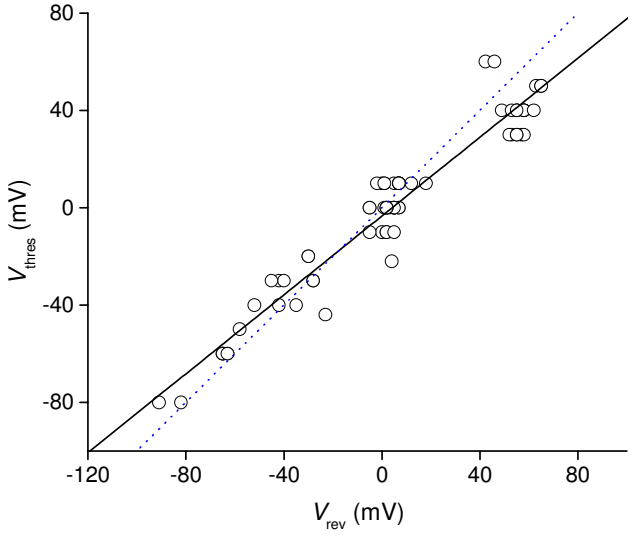

Figure 4.9. **V_{thres} to V_{rev} relationship.** V_{thres} for each cell is plotted against its V_{rev} (mean ± S.E.M.) along different pH solutions. The dotted line represents the equality V_{thres} = V_{rev}. The straight line shows the least square linear fitting with V_{thres} = 0.81 V_{rev} – 3.4. n = 32 cells.

The linear dependence obtained for all data plotted in **Figure 4.9** is:

$$V_{thres} = 0.81\, V_{rev} - 3.4 \text{ mV}$$

(Equation 4.4)

From **Equation 4.4**, the line predicts a V_{thres} shift of approximately 47 mV per unit of pH.

The threshold potential, determined experimentally as the smallest voltage value where it was possible to distinguish a characteristic tail current during repolarization, is claimed to be ~ 1 % of the maximum g_H [7] and has been demonstrated to shift ~ 40 mV when the pH gradient across the membrane changes in one unit [70], [93], [90], being slightly higher for the case of NpH_V1.

Table 4.2 depicts a summary of the values reported in similar whole cell studies and the one estimated for NpH_V1.

Table 4.2. **pH dependence of gating for proton channels reported in different whole-cell studies.**

Cell type	Slope	Offset (mV)	Reference
Nicoletia phytophila	0.81	- 3.4	[64]
Rat alveolar epithelium	0.76	18	[90]
Karlodinium veneficum	0.79	-37	[7]
HEK-293 endogenous currents	0.71	27	[70]
HEK-293 or COS-7 co-transfected with WT hH_V1 and GFP	0.66	-16	[70]
WT hH_V1 in HEK293	0.82	14	[3]
Native proton currents (15 cell types)	0.79	23	[5]

NpH_V1 slope is comparable with the 0.82 value reported by Ramsey *et al.* for the human channel. However, a more general comparison could be done with the slope reported by DeCoursey [5] where the author estimated a general equation from a pool of 15 different native proton currents, with a resulting slope of 0.79. The same value was reported years later when proton channels were discovered in dinoflagellates [7]. Moreover, even less steeper slopes have been described in the case of expressed proton channels which present a V_{thres} more negative than the + 20 mV for native channels [70].

The slope of 0.81 calculated for NpH_V1 points out to a slightly altered pH-dependent gating, compared with the 40 mV / unit of pH dogma proposed for proton channels [2]. In other words, the gating in NpH_V1 changes more when pH_i or pH_o are altered.

Furthermore, under different pH_i (5.5, 6.5 and 7.5) and pH_o (4.5 to 8.0) conditions, results indicate that this pH-dependent gating in NpH_V1 is dependent on the pH gradient across the membrane but not on the absolute pH_i or pH_o values. This fact is another well-known feature for proton channels [93].

The obtained offset of -3.4 mV reveals that NpH_V1 could present inward proton currents at symmetrical pH_i/pH_o and with more probability under an inward proton gradient environment ($pH_i > pH_o$). In this sense, during some measurements it was possible to observe inward currents during depolarizing pulses due to a V_{thres} more negative than V_{rev}. This can be seen in the data located under the dotted line of **Figure 4.9.** A more negative offset has been reported previously for expressed proton channels which has been explained as a result of a negative shift in the absolute voltage dependence of gating [70]. The extreme case has been shown by kH_V1 which displays a well negative offset of – 37 mV. The net result of this negative offset in the presence of consistent inward proton currents along a wide range of pH [7]. Compared to both cases, NpH_V1 exhibit a more positive g_H activation.

When comparing to other H_V1, NpH_V1 shows bigger differences in the offset than in the slope. This is an indicative that the pH sensing mechanism should be the same for *Nicoletia phytophila* and the rest of proton channels. The phenomena agrees with results presented by Ramsey *et al.* were an evaluation of 30 different hH_V1 mutant channels brought variations of > 200 mV in the offset but without a significant changes in slope [85].

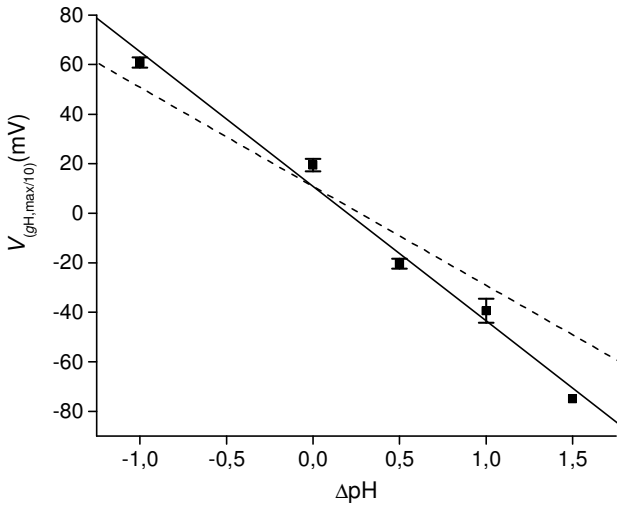

Figure 4.10. **10 % of $g_{H,max}$ against ΔpH plot.** The voltage corresponding to a 10 % of the maximum proton conductance for each cell is plotted against the pH gradient across the membrane (mean ± S.E.M.), where ΔpH = pH_o – pH_i and n = 32 cells. The dotted line shows the 40 mV per unit of pH rule. The straight line is the least square linear fitting of the data, resulting in a slope of -54 mV per unit of pH.

In order to study more in detail this slightly divergence between NpH_V1 and the 40 mV / unit of pH dogma, 10 % of the maximal proton conductance was plotted against the pH gradient across the membrane (**Figure 4.10**). This strategy allows a direct comparison of g_H – voltage shifts with their prediction accordingly with the "rule of forty" (*dotted line in* **Figure 4.10**). In addition, choosing a 10 % of maximal g_H avoids forcing non-sigmoidal g_H-V curves to fit a Boltzmann function.

The analysis done with this second method showed a shift of 54 mV / pH unit in the g_H – V curve, bigger than 40 mV / pH and even bigger than the value obtained with the linear regression analysis of the V_{thres} – V_{rev} plot.

With both methodologies, NpH_V1 demonstrated to have an enhanced pH – dependent gating when compared to other protons channels. However, how NpH_V1 and the rest of proton channel sense pH variations and which amino acid or amino acids are responsible for it, is still unknown.

In this way, charged amino acids prone to be protonated or deprotonated are good candidates when looking for a pH sensor. The alignment done (**Figure 4.2**) showed conservation of most of all charged residues in NpH_V1 and in all other species. Therefore, it seems to be logic not to consider those amino acids responsible of the slightly modulated pH sensing in NpH_V1.

On the other hand, polar amino acids as Asn, Gln, Cys, Tyr and Ser could be good candidates to explain enhanced pH sensing or even hydrophobic residues able to restrict water accessibility to protonation sites. It has been reported before that pk_a values of hydrophobic amino acids can change depending if they are fully or partially embedded in the lipid membrane [122]–[124].

In summary, NpH_V1 showed pH-dependent gating as all H_V1 known, but with an increased pH sensing. Further detailed studies in NpH_V1 could be useful for helping to solve the remaining mystery about the pH-sensor of the voltage-gated proton channel.

4.7 Is the Asp in the middle of S1 the selectivity filter for NpH_V1 as well?

Possibly the main characteristic of H_V1 is its extremely high proton selectivity.

Despite the existence of different proposals describing the molecular mechanism for protons conduction, it is clear that an aspartate residue in the middle of the S1 segment plays a major role in the general mechanism of selectivity. This amino acid is found consistently in all proton channels studied so far, residing as the selectivity

filter of the channel. Punctually and consequently with previous studies, this function has been attributed to Asp112 for humans [49] and to Asp51 for *Karlodinium veneficum* [7]

In accordance with the alignment in **Figure 4.11**, Asp66 in NpH_V1 has all the characteristics of a suitable candidate as the selectivity filter.

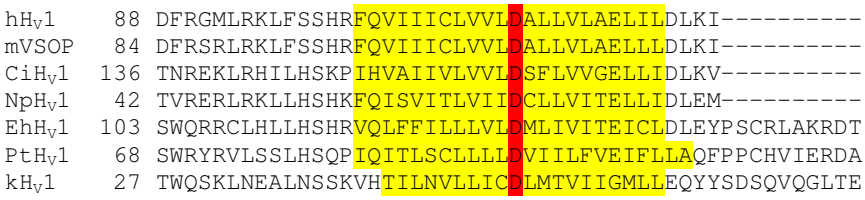

Figure 4.11. **Alignment on S1 for different H_V1 showing the preserved aspartate in the middle of the segment.** hH_V1 = human, mVSOP = mouse, CiH_V1 = *Ciona intestinalis*, NpH_V1 = *Nicoletia phytophila*, EhH_V1 = *Emiliana huxleyi*, PtH_V1 = *Phaeodactylum tricornutum,* kH_V1 = *Karlodinium veneficum*. The yellow color highlights the S1 segment and the red color the conserved aspartate residue in the middle of the segment.

In order to prove if Asp66 is the selectivity filter, Asp66 was mutated in Ala, Ser, His and Glu as in previous selectivity filter studies [7], [49]. The experiment consists in exchanging the dominant ion TMA^+ $CH_3SO_3^-$ from the external solution to TMA^+ Cl^- and performing tail current measurements in both conditions, at symmetrical pH 5.5. Then, comparing the results with the predicted E_H allows to test proton selectivity. Any ion permeation different than protons would produce a variation of V_{rev}.

If chloride would be better permeable than $CH_3SO_3^-$, then this could produce not only a shift in V_{rev} but also generate bigger currents in the current families.

Substitutions to an acidic amino acid

In the experiments done and as it can be seen in **Figure 4.12**, there were no significant changes in the conduction of the channel (**Figure 4.12 A**) when Asp66 was mutated to the negatively charged glutamic acid (pK_a = 4.07).

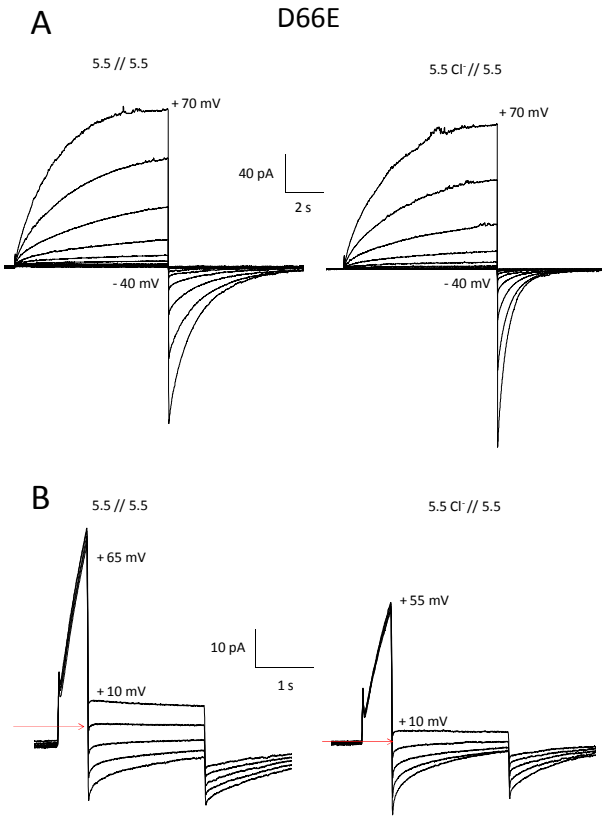

Figure 4.12. **D66E mutant.** A) Family of pulses from -30 mV up to + 70 mV in whole-cell configuration, with 10 mV increments, holding potential of – 40 mV and at pH 5.5 symmetrical conditions. Left: $CH_3SO_3^-$ as dominant anion, right: Cl^- as dominant anion. B) Tail current measurements from pH_o = 5.5 $CH_3SO_3^-$ (left) to pH_o = 5.5 Cl^- (right), obtained by a pre-pulse of + 65 mV (left) and + 55 mV (right) and a test pulse in 10 mV increments. The V_{rev} is highlighted by an arrow.

Current amplitudes at V_{test} = + 70 mV were basically the same when $CH_3SO_3^-$ was the dominant ion and when it was substituted by Cl^-. Small current differences are attributed to cell depletion during measurements and may not represent anion permeation.

In addition, analysis of tail currents indicates a V_{rev} of ~ 0 mV in TMA^+ $CH_3SO_3^-$ and V_{rev} of ~ +5 mV in TMA^+ Cl^- (**Figure 4.12 B**). This matches almost the value for the calculated liquid junction potential (LJP) if $CH_3SO_3^-$ is exchanged for Cl^-.

The exchange of $CH_3SO_3^-$ to Cl^- didn´t change the currents, therefore it can be concluded that proton selectivity did not change. D66E mutant behaves as WT.

Substitutions to non-acidic amino acids

An opposite result was obtained when aspartate was mutated to non-acidic amino acids. Measurements from D66H, D66A and D66S showed clear Cl^- permeation through the channel. Among the three mutants, Ser mutant presented the biggest V_{rev} shift with a mean value of – 47 mV in 7 cells (**Figure 4.13 B**).

Currents at symmetrical pH 5.5 TMA^+ $CH_3SO_3^-$ were small (**Figure 4.13 A, left**) but still reversing close to 0 mV (**Figure 4.13 B, left**). In addition, these currents were also smaller than WT when $CH_3SO_3^-$ was the dominant anion.

As it has been mentioned before, the effect of the greater Cl^- permeation over $CH_3SO_3^-$ can be seen during the family of pulses (**Figure 4.13 A**). When all the external $CH_3SO_3^-$ was replaced with Cl^-, outward currents increased considerably, more than four times at the same depolarization, in accordance with Cl^- influx. The current increment once Cl^- is the dominant ion indicates higher permeability in comparison with $CH_3SO_3^-$. These results are in agreement with what Musset *et al.*

[49] have reported in 2011 for the same mutant in the human channel based on V_{rev} variations, where a relative permeability $P_{CH_3SO_3^-}/P_{Cl}$ of 0.15 was determined.

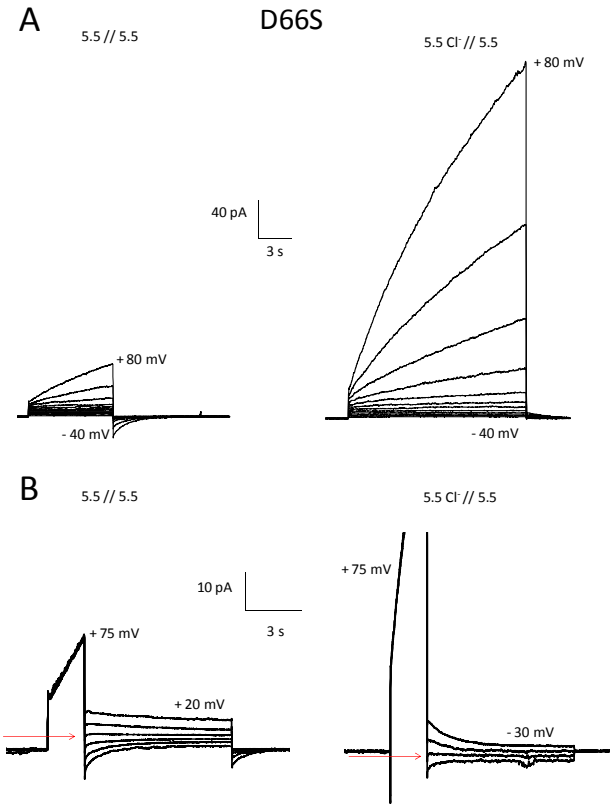

Figure 4.13. **D66S mutant.** A) Family of pulses from -30 mV up to + 80 mV in whole-cell configuration, with 10 mV increments, holding potential of – 40 mV and at symmetrical pH 5.5. Left: $CH_3SO_3^-$ as dominant anion, right: Cl^- as dominant anion depicting outward tail currents. B) Tail current measurements from pH_o = 5.5 $CH_3SO_3^-$ (left) to pH_o = 5.5 Cl^- (right), obtained by a pre-pulse of + 75 mV plus a second pulse with 10 mV increments. V_{rev} is highlighted with an arrow.

In addition, presence of outward tail currents at -40 mV can be seen in the family of pulses at pH 5.5 Cl^- (*see* **Figure 4.13.A, right**).

Since an individual ionic current is defined by Ohm's Law as

$$I_i = g_i(E_m - E_i)$$

(Equation 4.2)

where

I_i = ionic current of the species i

g_i = conductance of the ion i

E_m = membrane potential

E_i = equilibrium potential for i

positive values or outward currents are obtained only when $E_m > E_i$. In this sense, considering a membrane potential of -40 mV (V_{hold}), the equilibrium potential must be more negative than this value, in fact, ~ - 47 mV.

Here both, tail current measurements and the appearance of outward tail components during depolarizing protocols, clearly indicate a shift on V_{rev}. This effect on the reversal potential implies that the channel is no longer proton selective.

Because in the experiments the proton concentration outside and inside the cell is the same, V_{rev} should be close 0 mV in cases where proton selectivity remains (D66E and WT), doesn´t matter which is the dominant anion: $CH_3SO_3^-$ or Cl^-. Then, a shift in the equilibrium potential must be attributed to any other ion passing through the channel.

In the assays, all the ions were present at the same concentration inside and outside the cell (*see* **Equation 4.1**), except when Cl^- substituted $CH_3SO_3^-$. This substitution generates an inward electrochemical driving force that shifts V_{rev} negatively in case of proton selectivity loss.

Another valid question here is if Asp neutralization makes the channel permeable just to anions or if by the other hand, cations as TMA^+ are able pass through as well.

Experiments where isotonic sucrose is used to determine anion against cation selectivity have been applied before [91]. In this approach, sucrose dilutes all the extracellular ions except H^+ and OH. In accordance with Nernst equation, a V_{rev} negative shift is obtained for cation selective channels and a positively shifts appears for anion selective ones. The strategy has been applied before by Musset *et al.* in their study about the selectivity filter of the human H_V1. In their work, D112A, D112H and D112S all have shown positive V_{rev} shifts, concluding that these mutants transform the proton channel into a mainly anion channel, where protons still could pass through [49].

A summary of measured V_{rev} for Asp66 mutants is shown in **Figure 4.14**.

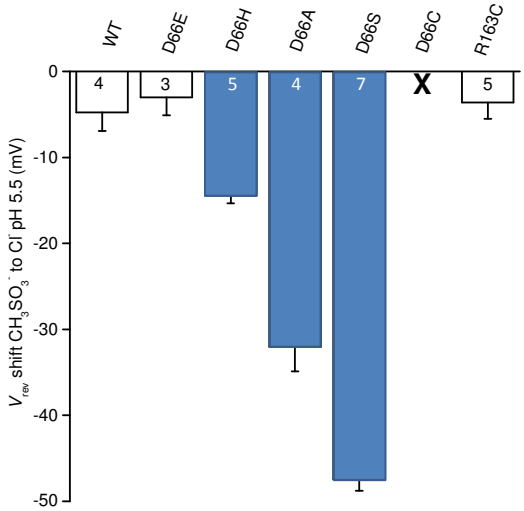

Figure 4.14. **Mutations of Asp66.** Reversal potentials corrected for LJP of different substitutions on position 66 (mean ± S.E.M). Blue bars represent those cases where chloride permeation was detectable as significant shift on V_{rev}. V_{rev} determination for D66C mutant was not possible due to its lacking of clear conduction (n = 5). Numbers on the bars represent the number of cells tested for each mutant.

The results demonstrate that substitutions to negatively charged residues, Asp (WT) and Glu, retain proton selectivity with minor variations of V_{rev} when compared with E_H. On the other hand, mutations to neutral amino acids lead to proton selectivity loss.

Among the non-proton selective channels, the biggest V_{rev} shift was detected for serine substitutions, ~ - 47 mV, then it could be concluded that this mutant shows the highest chloride permeability. The same big shift has been reported before for the corresponding mutants in kH_V1 and hH_V1.

A more moderate chloride permeability, around - 33 mV, was determined for D66A mutant, similar to – 29 mV determined for D112A in the human channel [49].

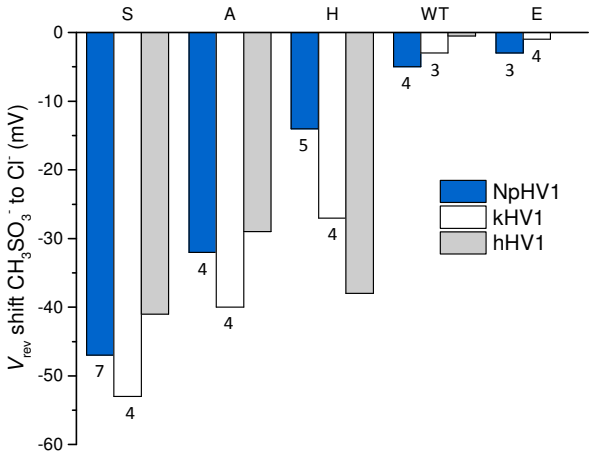

Figure 4.15. **Comparative V_{rev} shifts for selectivity filter mutations of different H_V1.** Reversal potentials corrected for LJP of different substitutions on Asp66 (NpH_V1), Asp51 (kH_V1) and Asp112 (hH_V1) at symmetrical pH 5.5. The number of measurements reported is shown below the bars; in the case of hH_V1 a n = 3 – 8 has been reported for the same mutations [49].

Finally a fewer shift of - 14 mV was identified for D66H mutants, even smaller than the – 27 mV reported for D51H in kH_V1[7].

The results are in agreement with the only two studies of this kind done up to date (**Figure 4.15**), showing a similar trend respecting to chloride permeability of the tested mutants.

Figure 4.15 shows V_{rev} shifts for Asp66 mutants in *Nicoletia* in comparison to same studies for humans and dinoflagellates.

It has been proposed before for CiH_V1 that Asp to Cys (D160C) mutation leads to a non-conducting channel [69].

Along 5 cells tested, results indicated that mutant D66C effectively lacks of clear conduction.

The recorded signals showed currents of less than 10 pA at + 100 mV as shown in **Figure 4.16**, making them impossible to resolve and therefore, to define as proton currents.

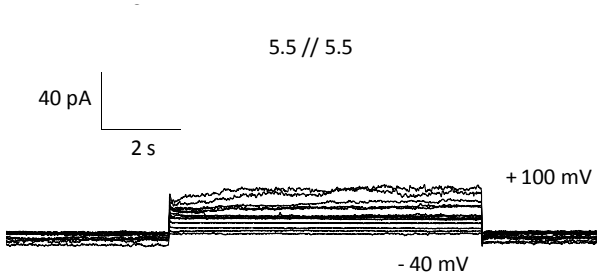

Figure 4.16. **D66C mutant typical whole-cell measurement.** Pulses from -30 mV up to + 100 mV in whole-cell configuration, in 10 mV increments, with a holding potential of – 40 mV and at symmetrical pH 5.5.

But, why is the proton selectivity lost when substituting Asp66 to neutral amino acids?

A possible explanation is brought by Dudev *et al.*[80]. In their quantum model, the authors evaluated salt bridge interactions between one of the argenines of S4 and the aspartate in S1. The charge interaction between both amino acids generates an energetic barrier in a narrow region of the channel pore.

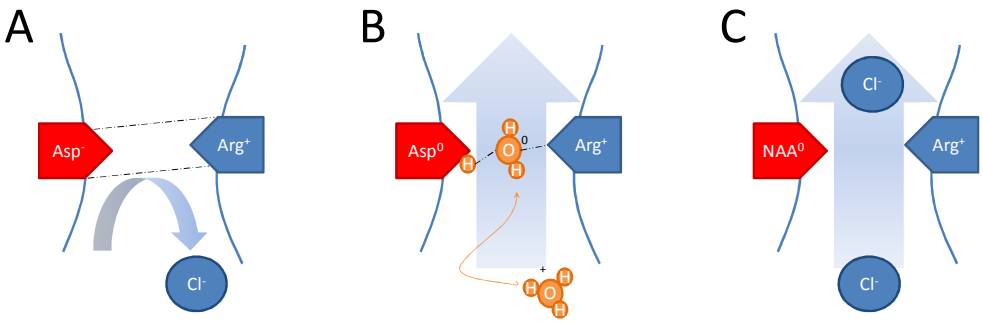

Figure 4.17. **Selectivity mechanism based on Dudev *et. al* study.** A) Energetic barrier formed by means of salt bridge interaction between Asp66 and Arg161, where Cl^- is not able to break it and therefore it is repulsed. B) Hydronium ion protonates Asp66 and coordinates in between with Arg161. A stable complex which breaks the energetic barrier is formed, allowing proton hopping to the other side of the bottle neck. C) Substitutions to non-acidic amino acid (NAA) implies an elimination of the energetic barrier and consequently, the repulsion for Cl^- is removed.

Basically, only hydronium is able to place in between both residues for protonating the aspartate. The resultant water molecule is coordinated then by the positively charged arginine (**Figure 4.17 B**). Both processes happen at the same time and create a favorable Asp^0-H_2O-Arg^+ interaction, breaking the energetic barrier. Afterwards, the proton can hop off from the Asp to another water molecule located in the other side of the bottle neck, resulting in a recovery of the Asp^- - Arg^+ barrier.

All other ions resulting in a Asp^- - X^-/X^+ - Arg^+ interaction demonstrated to be unfavorable [80]. In the open state, other ions as Cl^- or Na^+ are firstly repulsed by the amino acid with the same charge, Arg in the case of Na^+ and Asp in the case of Cl^-. The repulsion will then push the ion towards the other amino acid with opposite charge. In the process, the Asp – Arg barrier is partially restored and closes the pathway for other ions [80].

The same behavior was seeing during the experiments with NpH_V1.

Considering a working pH of 5.5 and the pk_a values presented in **Table 4.3**, Ala, His, Ser and Cys are protonated at those pH conditions and consequently, neutralized.

When Asp66 was substituted to these amino acids, the negative charge is eliminated and thus the interaction with the positive charge on S4 broken. The energetic barrier does not longer exist.

Table 4.3. **Acid dissociation constants and isoelectric point of amino acids used for chloride permeation experiments.**

Amino acid	**pk_1 -COOH**	**pk_2 $-NH_3^+$**	**pk_a R group**	**pI**
Asp	1.88	9.60	3.65	2.77
Glu	2.19	9.67	4.25	3.22
Ala	2.34	9.69	-	6.01
His	1.82	9.17	6.00	7.59
Ser	2.21	9.15	-	5.58
Cys	1.96	10.28	8.18	5.07

Adopted from Table 3-1 [125].

Once this barrier is disrupted, other ions different than H^+, e.g. Cl^- or Na^+, can pass through (**Figure 4.17 C**), provoking a shift in the V_{rev} measured.

The effect couldn't be seen on Cys substitutions due to the lacking of clear conduction; however, it is expected to present the same behavior.

On the other hand, both Asp and Glu remain deprotonated at pH 5.5. The electrostatic interaction with R2 keeps going on and the energetic barrier continue ruling the selectivity process. Here, all ions except hydronium are rejected (**Figure 4.17 A and B**). Then, the channel continues being proton selective without significant shifts on V_{rev}.

In conclusion, the essays demonstrated that Asp66 is the selectivity filter for NpH_V1, in agreement with the general selectivity mechanism for proton channels and with the hydrogen HBC classical theory proposed by Nagle and Morowitz [79], [126].

Role of the third arginine in S4: is it significant for proton selectivity in NpH_V1?

Despite the existence of a X-ray structure for the close state of H_V1 [50], an open state counterpart able to elucidate several enigmas about function and structure, is still missing.

Several studies pointing out to clarify the proton conduction pathway have been done [61], [68], [69], [71]–[73], [80], [115], [127]. In all of them it seems widely accepted that an arginine residue in the preserved VSD motif (R-x-W-R-x-x-R) plays an important role in proton conduction.

As common agreement, positive charged arginines (R1, R2, R3) from the VSD are responsible for voltage sensing, resulting in an upward movement of the S4 segment and allowing an open state configuration.

During the open state, interaction of the selectivity filter with one of the argenines from S4 establish the proton conduction pathway [68], [71], [80], [128].

In this direction, divided opinions can be found in the literature around which of those Arg interacts with the Asp on S1. Hence, a group of scientist defend the thesis of an R2D model meanwhile others support the idea of a R3D interaction (**Figure 4.18**).

In accordance with the alignment done, R163 in NpH_V1 shows homology with the R3 of other H_V1 (**Figure 4.19**). Therefore, cysteine substitutions on position 163 were done in order to verify the R3D hypothesis.

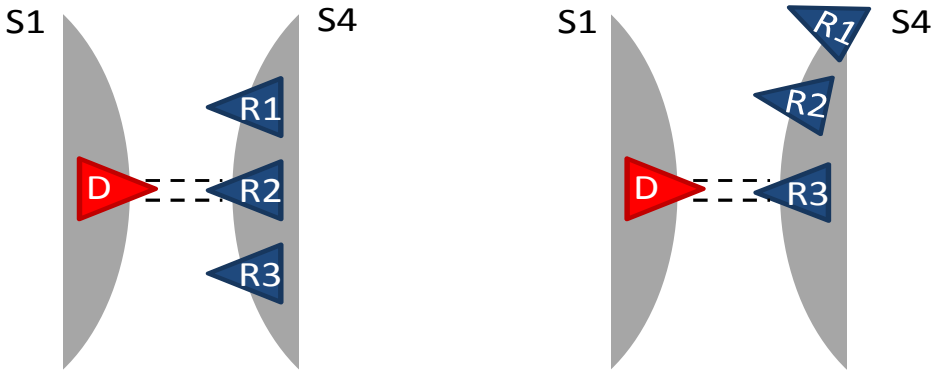

Li *et al.*, 2015 [61].

Morgan *et al.*, 2013 [73].

Kulleperuma *et al.*, 2013 [71].

Dudev *et al.*, 2015 [80].

Sakata *et al.*, 2010 [115].

Wood *et al.*, 2011 [72].

Chamberlin *et al.*, 2015 [69].

Mony *et al.*, 2015 [68].

Berger *et al.*, 2011 [128].

Figure 4.18. **Asp - Arg interaction during the open state configuration**. Left column: some of R2D model supporters. Right column: some of R3D model supporters.

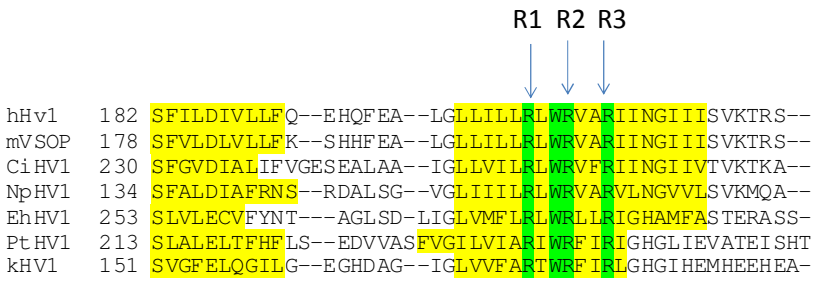

Figure 4.19. **R-x-W-R-x-x-R motif of different H_V1.** Part of the alignment done on S4 presenting the signature sequence RxWRxxR of different H_V1. Arginine R1, R2 and R3 are highlighted in green together with a conserved tryptophan.

Figure 4.20 shows a representative measurement for a R163C mutant. Here, whole-cell records along five cells exhibited consistent currents but with smaller amplitude than WT.

In addition, no current increments displaying Cl^- over $CH_3SO_3^-$ permeation were detected during the exchange; currents at the same test pulse were basically the same (**Figure 4.20 A**).

Moreover, recorded currents reverse close to 0 mV when chloride was the dominant anion (**Figure 4.20 B**), indicating proton selectivity retention (**Figure 4.14**).

Both, the lacking of significant differences in current amplitudes and reversal potentials indicate that the third argenine is not imperative for proton selectivity in NpH_V1, at least when pH_i and pH_o are equal to 5.5.

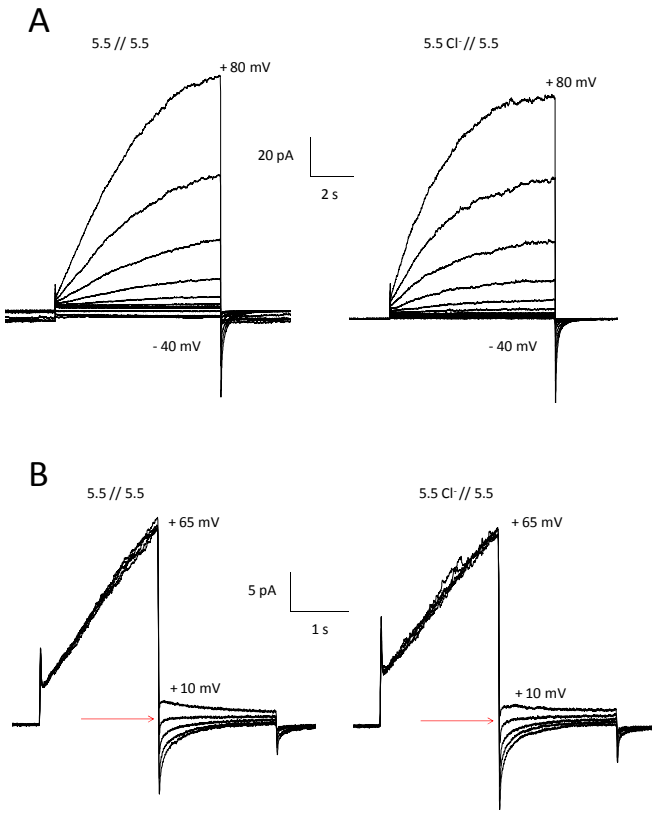

Figure 4.20. **R163C mutant.** A) Family of pulses from -30 mV up to + 80 mV in whole-cell configuration, with 10 mV increments, holding potential of – 40 mV and at pH 5.5 symmetrical conditions. Left: $CH_3SO_3^-$ as dominant anion, right: Cl^- as dominant anion. B) Tail current measurements from pH_o = 5.5 $CH_3SO_3^-$ (left) to pH_o = 5.5 Cl^- (right), obtained by a pre-pulse of + 65 mV plus a second pulse with 10 mV increments. The V_{rev} is highlighted by an arrow.

4.8 Final discussion

The special characteristics of the voltage-gated proton channel make it an important part in processes where acidification of the cell is produced, allowing a fast and efficient proton extrusion that recovers pH homeostasis. Perhaps because of this, it seems that H_V1 has been found in several single-celled organisms and in more complex species. Only one gene per species has been described so far.

Despite all reports of H_V1 genes in different species, only few of them have been confirmed by electrophysiological measurements. Common transcriptome sequence analysis has been used for detecting proton channels through Animalia kingdom but failed before for insects.

NpH_V1 is the first report of a proton channel in insects. Furthermore, it has been electrophysiologically characterized. When comparing NpH_V1 with other proton channels, it shows higher homology with the human and mouse proteins than with marine species (**Figure 4.21**). It presents a 33 % of homology with the human channel.

	hHv1	mVSOP	CiHv1	NpHv1	EhHv1	PtHv1	kHv1
hH_V1	0.0000	0.3804	2.2140	1.7007	3.1230	3.5424	3.1285
mVSOP	0.3804	0.0000	2.1943	1.7586	3.0425	3.4669	3.0559
CiH_V1	2.2140	2.1943	0.0000	2.0387	3.6584	3.2942	2.9904
NpH_V1	1.7007	1.7586	2.0387	0.0000	2.5216	3.4069	3.3261
EhH_V1	3.1230	3.0425	3.6584	2.5216	0.0000	2.8946	3.1580
PtH_V1	3.5424	3.4669	3.2942	3.4069	2.8946	0.0000	3.4430
kH_V1	3.1285	3.0559	2.9904	3.3261	3.1580	3.4430	0.0000

Figure 4.21. Phylogenetic matrix. Identity matrix of NpH_V1 compared with proton channels from other species are represented by arbitrary numbers. The higher the value is, the less identity between the channels. Values equal to 0 represent 100 % of identity. Results obtained by using PROTDIST (University of Washington, 2008).

H_V1 expression results in *T. domestica,* a common Zygentoma, showed a general distribution along the insect body: malphigian tubules, nervous and muscle tissue [64]; without a clear predilection for any. In insects, immune cells are located in the hemolymph which circulates around all insect´s body. Since proton channels are commonly related with immune system action [21], [48], [86], [128] – [131], it could be a reason why H_V1 seems to be expressed in all tested tissues. Moreover, H_V1 could be expressed on the tracheal system of the insect and because it traverses the whole body, it is another factor that should be considered.

Screening results of TSA databases showed positive results for H_V1 in the arthropods' subphylum, detected in chelicerata and crustaceans but not in myriapoda [64]. Proton channels were consistently found in basal insects and detected as well in some polyneopterans (walking sticks, mantids, earwings and crickets) [64], which could means the protein existence in higher insects as well. But why proton channels are commonly found in basal insects and not in the higher ones, is still unknown. Further studies represent a chance to clarify the evolution mechanisms of H_V1.

This work not only presents a new voltage-gated proton channel but additionally confirms general structural insights. Some of those characteristics demonstrated to be unaltered in NpH_V1 but other ones as the pH-dependent gating, is slightly modified. Further research focused on those small differences could elucidate important aspects of function and structure of protons channels that up to date remain unknown. As well, proton channels could be useful for resolving insect´s phylogeny aspects.

References

[1] B. Musset and T. DeCoursey, "Biophysical properties of the voltage gated proton channel HV1," *Wiley Interdiscip. Rev. Membr. Transp. Signal.*, vol. 1, no. 5, pp. 605–620, Sep. 2012.

[2] T. E. DeCoursey, "Voltage-gated proton channels: molecular biology, physiology, and pathophysiology of the H(V) family," *Physiol. Rev.*, vol. 93, no. 2, pp. 599–652, Apr. 2013.

[3] I. S. Ramsey, M. M. Moran, J. A. Chong, and D. E. Clapham, "A voltage-gated proton-selective channel lacking the pore domain," *Nature*, vol. 440, no. 7088, pp. 1213–1216, Apr. 2006.

[4] M. Sasaki, M. Takagi, and Y. Okamura, "A Voltage Sensor-Domain Protein Is a Voltage-Gated Proton Channel," *Science*, vol. 312, no. 5773, pp. 589–592, Apr. 2006.

[5] T. E. Decoursey, "Voltage-gated proton channels and other proton transfer pathways," *Physiol. Rev.*, vol. 83, no. 2, pp. 475–579, Apr. 2003.

[6] T. E. DeCoursey, "The Voltage-Gated Proton Channel: A Riddle, Wrapped in a Mystery, inside an Enigma," *Biochemistry (Mosc.)*, vol. 54, no. 21, pp. 3250–3268, Jun. 2015.

[7] S. M. E. Smith *et al.*, "Voltage-gated proton channel in a dinoflagellate," *Proc. Natl. Acad. Sci.*, vol. 108, no. 44, pp. 18162–18167, Jan. 2011.

[8] D.-Y. Cho, M. Hajighasemi, P. H. Hwang, B. Illek, and H. Fischer, "Proton secretion in freshly excised sinonasal mucosa from asthma and sinusitis patients," *Am. J. Rhinol. Allergy*, vol. 23, no. 6, pp. e10-13, Dec. 2009.

[9] H. Fischer, "Function of Proton Channels in Lung Epithelia," *Wiley Interdiscip. Rev. Membr. Transp. Signal.*, vol. 1, no. 3, pp. 247–258, 2012.

[10] H. Fischer, J. H. Widdicombe, and B. Illek, "Acid secretion and proton conductance in human airway epithelium," *Am. J. Physiol. Cell Physiol.*, vol. 282, no. 4, pp. C736-743, Apr. 2002.

[11] P. V. Lishko, I. L. Botchkina, A. Fedorenko, and Y. Kirichok, "Acid extrusion from human spermatozoa is mediated by flagellar voltage-gated proton channel," *Cell*, vol. 140, no. 3, pp. 327–337, Feb. 2010.

[12] B. Musset *et al.*, "NOX5 in human spermatozoa: expression, function, and regulation," *J. Biol. Chem.*, vol. 287, no. 12, pp. 9376–9388, Mar. 2012.

[13] Y. Okochi *et al.*, "The voltage-gated proton channel Hv1/VSOP inhibits neutrophil granule release," *J. Leukoc. Biol.*, vol. 99, no. 1, pp. 7–19, Jan. 2016.

[14] D. Morgan *et al.*, "Voltage-gated proton channels maintain pH in human neutrophils during phagocytosis," *Proc. Natl. Acad. Sci. U. S. A.*, vol. 106, no. 42, pp. 18022–18027, Oct. 2009.

[15] Y. Okochi, M. Sasaki, H. Iwasaki, and Y. Okamura, "Voltage-gated proton channel is expressed on phagosomes," *Biochem. Biophys. Res. Commun.*, vol. 382, no. 2, pp. 274–279, May 2009.

[16] A. Kapus, R. Romanek, A. Y. Qu, O. D. Rotstein, and S. Grinstein, "A pH-sensitive and voltage-dependent proton conductance in the plasma membrane of macrophages," *J. Gen. Physiol.*, vol. 102, no. 4, pp. 729–760, Oct. 1993.

[17] T. E. DeCoursey and V. V. Cherny, "Potential, pH, and arachidonate gate hydrogen ion currents in human neutrophils," *Biophys. J.*, vol. 65, no. 4, pp. 1590–1598, Oct. 1993.

[18] R. Murphy and T. E. DeCoursey, "Charge compensation during the phagocyte respiratory burst," *Biochim. Biophys. Acta*, vol. 1757, no. 8, pp. 996–1011, Aug. 2006.

[19] D. V. Gordienko, M. Tare, S. Parveen, C. J. Fenech, C. Robinson, and T. B. Bolton, "Voltage-activated proton current in eosinophils from human blood," *J. Physiol.*, vol. 496 (Pt 2), pp. 299–316, Oct. 1996.

[20] B. Musset, V. V. Cherny, and T. E. DeCoursey, "Strong glucose dependence of electron current in human monocytes," *Am. J. Physiol. Cell Physiol.*, vol. 302, no. 1, pp. C286-295, Jan. 2012.

[21] M. Capasso *et al.*, "HVCN1 modulates BCR signal strength via regulation of BCR-dependent generation of reactive oxygen species," *Nat. Immunol.*, vol. 11, no. 3, pp. 265–272, Mar. 2010.

[22] L. Bernheim, R. M. Krause, A. Baroffio, M. Hamann, A. Kaelin, and C. R. Bader, "A voltage-dependent proton current in cultured human skeletal muscle myotubes," *J. Physiol.*, vol. 470, pp. 313–333, Oct. 1993.

[23] B. Musset *et al.*, "A pH-stabilizing role of voltage-gated proton channels in IgE-mediated activation of human basophils," *Proc. Natl. Acad. Sci. U. S. A.*, vol. 105, no. 31, pp. 11020–11025, Aug. 2008.

[24] T. Nordström *et al.*, "Regulation of cytoplasmic pH in osteoclasts. Contribution of proton pumps and a proton-selective conductance," *J. Biol. Chem.*, vol. 270, no. 5, pp. 2203–2212, Feb. 1995.

[25] Q. Zhao *et al.*, "The voltage-gated proton channel Hv1 is expressed in pancreatic islet β-cells and regulates insulin secretion," *Biochem. Biophys. Res. Commun.*, vol. 468, no. 4, pp. 746–751, Dec. 2015.

[26] C. Eder and T. E. DeCoursey, "Voltage-gated proton channels in microglia," *Prog. Neurobiol.*, vol. 64, no. 3, pp. 277–305, Jun. 2001.

[27] C. Eder, H. G. Fischer, U. Hadding, and U. Heinemann, "Properties of voltage-gated currents of microglia developed using macrophage colony-stimulating factor," *Pflüg. Arch. Eur. J. Physiol.*, vol. 430, no. 4, pp. 526–533, Aug. 1995.

[28] E. Hondares *et al.*, "Enhanced activation of an amino-terminally truncated isoform of the voltage-gated proton channel HVCN1 enriched in malignant B cells," *Proc. Natl. Acad. Sci. U. S. A.*, vol. 111, no. 50, pp. 18078–18083, Dec. 2014.

[29] Y. Wang, S. J. Li, J. Pan, Y. Che, J. Yin, and Q. Zhao, "Specific expression of the human voltage-gated proton channel Hv1 in highly metastatic breast cancer cells, promotes tumor progression and metastasis," *Biochem. Biophys. Res. Commun.*, vol. 412, no. 2, pp. 353–359, Aug. 2011.

[30] Y. Wang, S. J. Li, X. Wu, Y. Che, and Q. Li, "Clinicopathological and biological significance of human voltage-gated proton channel Hv1 protein overexpression in breast cancer," *J. Biol. Chem.*, vol. 287, no. 17, pp. 13877–13888, Apr. 2012.

[31] Y. Wang, X. Wu, Q. Li, S. Zhang, and S. J. Li, "Human voltage-gated proton channel hv1: a new potential biomarker for diagnosis and prognosis of colorectal cancer," *PloS One*, vol. 8, no. 8, p. e70550, 2013.

[32] L. Ribeiro-Silva, F. O. Queiroz, A. M. B. da Silva, A. E. Hirata, and M. Arcisio-Miranda, "Voltage-Gated Proton Channel in Human Glioblastoma Multiforme Cells," *ACS Chem. Neurosci.*, vol. 7, no. 7, pp. 864–869, Jul. 2016.

[33] T. Seredenina, N. Demaurex, and K.-H. Krause, "Voltage-Gated Proton Channels as Novel Drug Targets: From NADPH Oxidase Regulation to Sperm Biology," *Antioxid. Redox Signal.*, vol. 23, no. 5, pp. 490–513, Aug. 2015.

[34] A. Fernandez, A. Pupo, K. Mena-Ulecia, and C. Gonzalez, "Pharmacological modulation of proton channel Hv1 in cancer therapy: Future perspectives," *Mol. Pharmacol.*, Jun. 2016.

[35] H. Shin, J. Kim, and J.-H. Song, "Clozapine and olanzapine inhibit proton currents in BV2 microglial cells," *Eur. J. Pharmacol.*, vol. 755, pp. 74–79, May 2015.

[36] M. Capasso, T. E. DeCoursey, and M. J. S. Dyer, "pH regulation and beyond: unanticipated functions for the voltage-gated proton channel, HVCN1," *Trends Cell Biol.*, vol. 21, no. 1, pp. 20–28, Jan. 2011.

[37] A. Pupo and C. Gonzalez León, "In pursuit of an inhibitory drug for the proton channel," *Proc. Natl. Acad. Sci. U. S. A.*, vol. 111, no. 27, pp. 9673–9674, Jul. 2014.

[38] K. Javor, J.-N. Tisserant, and A. Stemmer, "Biofuel cell operating on activated THP-1 cells: A fuel and substrate study," *Biosens. Bioelectron.*, vol. 87, pp. 1–6, Jan. 2017.

[39] R. C. Thomas and R. W. Meech, "Hydrogen ion currents and intracellular pH in depolarized voltage-clamped snail neurones," *Nature*, vol. 299, no. 5886, pp. 826–828, Oct. 1982.

[40] M. Fogel and J. W. Hastings, "Bioluminescence: mechanism and mode of control of scintillon activity," *Proc. Natl. Acad. Sci. U. S. A.*, vol. 69, no. 3, pp. 690–693, Mar. 1972.

[41] L. Byerly, R. Meech, and W. Moody, "Rapidly activating hydrogen ion currents in perfused neurones of the snail, Lymnaea stagnalis," *J. Physiol.*, vol. 351, pp. 199–216, Jun. 1984.

[42] M. E. Barish and C. Baud, "A voltage-gated hydrogen ion current in the oocyte membrane of the axolotl, Ambystoma," *J. Physiol.*, vol. 352, pp. 243–263, Jul. 1984.

[43] T. E. DeCoursey, "Hydrogen ion currents in rat alveolar epithelial cells.," *Biophys. J.*, vol. 60, no. 5, pp. 1243–1253, Nov. 1991.

[44] N. Demaurex, J. Schrenzel, M. E. Jaconi, D. P. Lew, and K. H. Krause, "Proton channels, plasma membrane potential, and respiratory burst in human neutrophils," *Eur. J. Haematol.*, vol. 51, no. 5, pp. 309–312, Nov. 1993.

[45] S.-Y. Lee, J. A. Letts, and R. MacKinnon, "Dimeric subunit stoichiometry of the human voltage-dependent proton channel Hv1," *Proc. Natl. Acad. Sci. U. S. A.*, vol. 105, no. 22, pp. 7692–7695, Jun. 2008.

[46] F. Tombola, M. H. Ulbrich, and E. Y. Isacoff, "The voltage-gated proton channel Hv1 has two pores, each controlled by one voltage sensor," *Neuron*, vol. 58, no. 4, pp. 546–556, May 2008.

[47] H. P. Koch, T. Kurokawa, Y. Okochi, M. Sasaki, Y. Okamura, and H. P. Larsson, "Multimeric nature of voltage-gated proton channels," *Proc. Natl. Acad. Sci. U. S. A.*, vol. 105, no. 26, pp. 9111–9116, Jul. 2008.

[48] I. S. Ramsey, E. Ruchti, J. S. Kaczmarek, and D. E. Clapham, "Hv1 proton channels are required for high-level NADPH oxidase-dependent superoxide production during the phagocyte respiratory burst," *Proc. Natl. Acad. Sci. U. S. A.*, vol. 106, no. 18, pp. 7642–7647, May 2009.

[49] B. Musset, S. M. E. Smith, S. Rajan, D. Morgan, V. V. Cherny, and T. E. DeCoursey, "Aspartate 112 is the selectivity filter of the human voltage-gated proton channel," *Nature*, vol. 480, no. 7376, pp. 273–277, Dec. 2011.

[50] K. Takeshita *et al.*, "X-ray crystal structure of voltage-gated proton channel," *Nat. Struct. Mol. Biol.*, vol. 21, no. 4, pp. 352–357, Apr. 2014.

[51] K. Castillo *et al.*, "Voltage-gated proton (H(v)1) channels, a singular voltage sensing domain," *FEBS Lett.*, vol. 589, no. 22, pp. 3471–3478, Nov. 2015.

[52] K. Takeshita, Y. Okamura, and A. Nakagawa, "[Structural insight into the regulation mechanism of proton leakage based on crystal structure of voltage-gated proton channel (VSOP)]," *Seikagaku*, vol. 87, no. 5, pp. 625–628, Oct. 2015.

[53] A. El Chemaly, Y. Okochi, M. Sasaki, S. Arnaudeau, Y. Okamura, and N. Demaurex, "VSOP/Hv1 proton channels sustain calcium entry, neutrophil migration, and superoxide production by limiting cell depolarization and acidification," *J. Exp. Med.*, vol. 207, no. 1, pp. 129–139, Jan. 2010.

[54] B. Musset *et al.*, "Zinc inhibition of monomeric and dimeric proton channels suggests cooperative gating," *J. Physiol.*, vol. 588, no. Pt 9, pp. 1435–1449, May 2010.

[55] B. Musset, S. M. E. Smith, S. Rajan, V. V. Cherny, D. Morgan, and T. E. DeCoursey, "Oligomerization of the voltage-gated proton channel," *Channels Austin Tex*, vol. 4, no. 4, pp. 260–265, Aug. 2010.

[56] S. J. Li, Q. Zhao, Q. Zhou, H. Unno, Y. Zhai, and F. Sun, "The role and structure of the carboxyl-terminal domain of the human voltage-gated proton channel Hv1," *J. Biol. Chem.*, vol. 285, no. 16, pp. 12047–12054, Apr. 2010.

[57] H. Okuda, Y. Yonezawa, Y. Takano, Y. Okamura, and Y. Fujiwara, "Direct Interaction between the Voltage Sensors Produces Cooperative Sustained Deactivation in Voltage-gated H+ Channel Dimers," *J. Biol. Chem.*, vol. 291, no. 11, pp. 5935–5947, Mar. 2016.

[58] T. E. DeCoursey, "Voltage-gated proton channels find their dream job managing the respiratory burst in phagocytes," *Physiol. Bethesda Md*, vol. 25, no. 1, pp. 27–40, Feb. 2010.

[59] B. Musset *et al.*, "Identification of Thr29 as a critical phosphorylation site that activates the human proton channel Hvcn1 in leukocytes," *J. Biol. Chem.*, vol. 285, no. 8, pp. 5117–5121, Feb. 2010.

[60] A. Pupo, D. Baez-Nieto, A. Martínez, R. Latorre, and C. González, "Proton channel models filling the gap between experimental data and the structural rationale," *Channels Austin Tex*, vol. 8, no. 3, pp. 180–192, 2014.

[61] Q. Li *et al.*, "Resting state of the human proton channel dimer in a lipid bilayer," *Proc. Natl. Acad. Sci. U. S. A.*, vol. 112, no. 44, pp. E5926-5935, Nov. 2015.

[62] Y. Fujiwara and Y. Okamura, "Temperature-sensitive gating of voltage-gated proton channels," *Curr. Top. Membr.*, vol. 74, pp. 259–292, 2014.

[63] T. E. DeCoursey and J. Hosler, "Philosophy of voltage-gated proton channels," *J. R. Soc. Interface*, vol. 11, no. 92, p. 20130799, Mar. 2014.

[64] G. Chaves, C. Derst, A. Franzen, Y. Mashimo, R. Machida, and B. Musset, "Identification of an HV 1 Voltage-Gated Proton Channel in Insects," *FEBS J.*, Feb. 2016.

[65] C. Gonzalez, H. P. Koch, B. M. Drum, and H. P. Larsson, "Strong cooperativity between subunits in voltage-gated proton channels," *Nat. Struct. Mol. Biol.*, vol. 17, no. 1, pp. 51–56, Jan. 2010.

[66] C. Gonzalez, S. Rebolledo, M. E. Perez, and H. P. Larsson, "Molecular mechanism of voltage sensing in voltage-gated proton channels," *J. Gen. Physiol.*, vol. 141, no. 3, pp. 275–285, Mar. 2013.

[67] Q. Li *et al.*, "Structural mechanism of voltage-dependent gating in an isolated voltage-sensing domain," *Nat. Struct. Mol. Biol.*, vol. 21, no. 3, pp. 244–252, Mar. 2014.

[68] L. Mony, T. K. Berger, and E. Y. Isacoff, "A specialized molecular motion opens the Hv1 voltage-gated proton channel," *Nat. Struct. Mol. Biol.*, vol. 22, no. 4, pp. 283–290, Apr. 2015.

[69] A. Chamberlin, F. Qiu, Y. Wang, S. Y. Noskov, and H. P. Larsson, "Mapping the gating and permeation pathways in the voltage-gated proton channel Hv1," *J. Mol. Biol.*, vol. 427, no. 1, pp. 131–145, Jan. 2015.

[70] B. Musset *et al.*, "Detailed comparison of expressed and native voltage-gated proton channel currents," *J. Physiol.*, vol. 586, no. 10, pp. 2477–2486, May 2008.

[71] K. Kulleperuma *et al.*, "Construction and validation of a homology model of the human voltage-gated proton channel hHV1," *J. Gen. Physiol.*, vol. 141, no. 4, pp. 445–465, Apr. 2013.

[72] M. L. Wood, E. V. Schow, J. A. Freites, S. H. White, F. Tombola, and D. J. Tobias, "Water wires in atomistic models of the Hv1 proton channel," *Biochim. Biophys. Acta*, vol. 1818, no. 2, pp. 286–293, Feb. 2012.

[73] D. Morgan *et al.*, "Peregrination of the selectivity filter delineates the pore of the human voltage-gated proton channel hHV1," *J. Gen. Physiol.*, vol. 142, no. 6, pp. 625–640, Dec. 2013.

[74] F. Bezanilla, "The Voltage Sensor in Voltage-Dependent Ion Channels," *Physiol. Rev.*, vol. 80, no. 2, pp. 555–592, Jan. 2000.

[75] D. M. Starace and F. Bezanilla, “A proton pore in a potassium channel voltage sensor reveals a focused electric field,” *Nature*, vol. 427, no. 6974, pp. 548–553, Feb. 2004.

[76] D. M. Starace and F. Bezanilla, “Histidine scanning mutagenesis of basic residues of the S4 segment of the shaker k+ channel,” *J. Gen. Physiol.*, vol. 117, no. 5, pp. 469–490, May 2001.

[77] C. M. Armstrong and F. Bezanilla, “Currents related to movement of the gating particles of the sodium channels,” *Nature*, vol. 242, no. 5398, pp. 459–461, Apr. 1973.

[78] D. M. Starace, E. Stefani, and F. Bezanilla, “Voltage-dependent proton transport by the voltage sensor of the Shaker K+ channel,” *Neuron*, vol. 19, no. 6, pp. 1319–1327, Dec. 1997.

[79] J. F. Nagle and H. J. Morowitz, “Molecular mechanisms for proton transport in membranes,” *Proc. Natl. Acad. Sci.*, vol. 75, no. 1, pp. 298–302, Jan. 1978.

[80] T. Dudev *et al.*, “Selectivity Mechanism of the Voltage-gated Proton Channel, HV1,” *Sci. Rep.*, vol. 5, p. 10320, 2015.

[81] D. Iovannisci, B. Illek, and H. Fischer, “Function of the HVCN1 proton channel in airway epithelia and a naturally occurring mutation, M91T,” *J. Gen. Physiol.*, vol. 136, no. 1, pp. 35–46, Jul. 2010.

[82] T. E. DeCoursey, D. Morgan, B. Musset, and V. V. Cherny, “Insights into the structure and function of HV1 from a meta-analysis of mutation studies,” *J. Gen. Physiol.*, vol. 148, no. 2, pp. 97–118, Aug. 2016.

[83] X. Tao, A. Lee, W. Limapichat, D. A. Dougherty, and R. MacKinnon, “A gating charge transfer center in voltage sensors,” *Science*, vol. 328, no. 5974, pp. 67–73, Apr. 2010.

[84] V. V. Cherny, D. Morgan, B. Musset, G. Chaves, S. M. E. Smith, and T. E. DeCoursey, “Tryptophan 207 is crucial to the unique properties of the human voltage-gated proton channel, hHV1,” *J. Gen. Physiol.*, vol. 146, no. 5, pp. 343–356, Nov. 2015.

[85] I. S. Ramsey, Y. Mokrab, I. Carvacho, Z. A. Sands, M. S. P. Sansom, and D. E. Clapham, “An aqueous H+ permeation pathway in the voltage-gated proton channel Hv1,” *Nat. Struct. Mol. Biol.*, vol. 17, no. 7, pp. 869–875, Jul. 2010.

[86] V. V. Cherny, R. Murphy, V. Sokolov, R. A. Levis, and T. E. DeCoursey, “Properties of single voltage-gated proton channels in human eosinophils estimated by noise analysis and by direct measurement,” *J. Gen. Physiol.*, vol. 121, no. 6, pp. 615–628, Jun. 2003.

[87] T. Schilling, A. Gratopp, T. E. DeCoursey, and C. Eder, “Voltage-activated proton currents in human lymphocytes,” *J. Physiol.*, vol. 545, no. Pt 1, pp. 93–105, Nov. 2002.

[88] N. Demaurex, S. Grinstein, M. Jaconi, W. Schlegel, D. P. Lew, and K. H. Krause, “Proton currents in human granulocytes: regulation by membrane potential and intracellular pH,” *J. Physiol.*, vol. 466, pp. 329–344, Jul. 1993.

[89] T. E. DeCoursey and V. V. Cherny, “Na(+)-H+ antiport detected through hydrogen ion currents in rat alveolar epithelial cells and human neutrophils,” *J. Gen. Physiol.*, vol. 103, no. 5, pp. 755–785, May 1994.

[90] T. E. DeCoursey and V. V. Cherny, "Deuterium Isotope Effects on Permeation and Gating of Proton Channels in Rat Alveolar Epithelium," *J. Gen. Physiol.*, vol. 109, no. 4, pp. 415–434, Apr. 1997.

[91] P. H. Barry, "The reliability of relative anion-cation permeabilities deduced from reversal (dilution) potential measurements in ion channel studies," *Cell Biochem. Biophys.*, vol. 46, no. 2, pp. 143–154, 2006.

[92] T. E. DeCoursey and V. V. Cherny, "Temperature dependence of voltage-gated H+ currents in human neutrophils, rat alveolar epithelial cells, and mammalian phagocytes," *J. Gen. Physiol.*, vol. 112, no. 4, pp. 503–522, Oct. 1998.

[93] V. V. Cherny, V. S. Markin, and T. E. DeCoursey, "The voltage-activated hydrogen ion conductance in rat alveolar epithelial cells is determined by the pH gradient," *J. Gen. Physiol.*, vol. 105, no. 6, pp. 861–896, Jun. 1995.

[94] A. L. Hodgkin and A. F. Huxley, "The components of membrane conductance in the giant axon of Loligo," *J. Physiol.*, vol. 116, no. 4, pp. 473–496, Apr. 1952.

[95] M. P. Mahaut-Smith, "The effect of zinc on calcium and hydrogen ion currents in intact snail neurones," *J. Exp. Biol.*, vol. 145, pp. 455–464, Sep. 1989.

[96] V. V. Cherny and T. E. DeCoursey, "pH-dependent inhibition of voltage-gated H(+) currents in rat alveolar epithelial cells by Zn(2+) and other divalent cations," *J. Gen. Physiol.*, vol. 114, no. 6, pp. 819–838, Dec. 1999.

[97] A. R. Taylor, C. Brownlee, and G. L. Wheeler, "Proton channels in algae: reasons to be excited," *Trends Plant Sci.*, vol. 17, no. 11, pp. 675–684, Nov. 2012.

[98] J. D. Rodriguez *et al.*, "Characterization and Subcellular Localization of Hv1 in Lingulodinium Polyedrum Confirms its Role in Bioluminescence," *Biophys. J.*, vol. 108, no. 2, p. 425a, Jan. 2015.

[99] B. Misof *et al.*, "Phylogenomics resolves the timing and pattern of insect evolution," *Science*, vol. 346, no. 6210, pp. 763–767, Nov. 2014.

[100] S. M. Thompson, "Relations between chord and slope conductances and equivalent electromotive forces," *Am. J. Physiol.*, vol. 250, no. 2 Pt 1, pp. C333-339, Feb. 1986.

[101] C. Gille and P. N. Robinson, "HotSwap for bioinformatics: a STRAP tutorial," *BMC Bioinformatics*, vol. 7, p. 64, 2006.

[102] D. Simm, K. Hatje, and M. Kollmar, "Waggawagga: comparative visualization of coiled-coil predictions and detection of stable single α-helices (SAH domains)," *Bioinforma. Oxf. Engl.*, vol. 31, no. 5, pp. 767–769, Mar. 2015.

[103] O. P. Hamill, A. Marty, E. Neher, B. Sakmann, and F. J. Sigworth, "Improved patch-clamp techniques for high-resolution current recording from cells and cell-free membrane patches," *Pflüg. Arch. Eur. J. Physiol.*, vol. 391, no. 2, pp. 85–100, Aug. 1981.

[104] T. E. DeCoursey, "Voltage-gated proton channels: what' next?," *J. Physiol.*, vol. 586, no. Pt 22, pp. 5305–5324, Nov. 2008.

[105] E. Neher, "Correction for liquid junction potentials in patch clamp experiments," *Methods Enzymol.*, vol. 207, pp. 123–131, 1992.

[106] A. R. Taylor, A. Chrachri, G. Wheeler, H. Goddard, and C. Brownlee, "A Voltage-Gated H + Channel Underlying pH Homeostasis in Calcifying Coccolithophores," *PLOS Biol*, vol. 9, no. 6, p. e1001085, Jun. 2011.

[107] U. Omasits, C. H. Ahrens, S. Müller, and B. Wollscheid, "Protter: interactive protein feature visualization and integration with experimental proteomic data," *Bioinformatics*, p. btt607, Oct. 2013.

[108] K. Arnold, L. Bordoli, J. Kopp, and T. Schwede, "The SWISS-MODEL workspace: a web-based environment for protein structure homology modelling," *Bioinforma. Oxf. Engl.*, vol. 22, no. 2, pp. 195–201, Jan. 2006.

[109] E. F. Pettersen *et al.*, "UCSF Chimera--a visualization system for exploratory research and analysis," *J. Comput. Chem.*, vol. 25, no. 13, pp. 1605–1612, Oct. 2004.

[110] S. P. Venkatachalan, J. D. Bushman, J. L. Mercado, F. Sancar, K. R. Christopherson, and A. J. Boileau, "Optimized expression vector for ion channel studies in Xenopus oocytes and mammalian cells using alfalfa mosaic virus," *Pflugers Arch.*, vol. 454, no. 1, pp. 155–163, Apr. 2007.

[111] L. Douglas, A. Davies, J. Wratten, and A. C. Dolphin, "Do voltage-gated calcium channel alpha2delta subunits require proteolytic processing into alpha2 and delta to be functional?," *Biochem. Soc. Trans.*, vol. 34, no. Pt 5, pp. 894–898, Nov. 2006.

[112] M. F. Sheets, J. W. Kyle, S. Krueger, and D. A. Hanck, "Optimization of a mammalian expression system for the measurement of sodium channel gating currents," *Am. J. Physiol.*, vol. 271, no. 3 Pt 1, pp. C1001-1006, Sep. 1996.

[113] D. McHugh, E. M. Sharp, T. Scheuer, and W. A. Catterall, "Inhibition of cardiac L-type calcium channels by protein kinase C phosphorylation of two sites in the N-terminal domain," *Proc. Natl. Acad. Sci.*, vol. 97, no. 22, pp. 12334–12338, Oct. 2000.

[114] S. Jha, *Essential Ion Channel Methods*. Academic Press, 2010.

[115] S. Sakata *et al.*, "Functionality of the voltage-gated proton channel truncated in S4," *Proc. Natl. Acad. Sci. U. S. A.*, vol. 107, no. 5, pp. 2313–2318, Feb. 2010.

[116] M. A. E. M. van der Aa *et al.*, "Cellular Uptake of Cationic Polymer-DNA Complexes Via Caveolae Plays a Pivotal Role in Gene Transfection in COS-7 Cells," *Pharm. Res.*, vol. 24, no. 8, pp. 1590–1598, Aug. 2007.

[117] Y. W. Cho, J.-D. Kim, and K. Park, "Polycation gene delivery systems: escape from endosomes to cytosol," *J. Pharm. Pharmacol.*, vol. 55, no. 6, pp. 721–734, Jun. 2003.

[118] D. Lechardeur, A. S. Verkman, and G. L. Lukacs, "Intracellular routing of plasmid DNA during non-viral gene transfer," *Adv. Drug Deliv. Rev.*, vol. 57, no. 5, pp. 755–767, Apr. 2005.

[119] V. De-la-Rosa, E. Suárez-Delgado, G. E. Rangel-Yescas, and L. D. Islas, "Currents through Hv1 channels deplete protons in their vicinity," *J. Gen. Physiol.*, vol. 147, no. 2, pp. 127–136, Jan. 2016.

[120] Y. Okamura, Y. Fujiwara, and S. Sakata, "Gating Mechanisms of Voltage-Gated Proton Channels," *Annu. Rev. Biochem.*, vol. 84, no. 1, pp. 685–709, 2015.

[121] M. Pusch and E. Neher, "Rates of diffusional exchange between small cells and a measuring patch pipette," *Pflüg. Arch. Eur. J. Physiol.*, vol. 411, no. 2, pp. 204–211, Feb. 1988.

[122] J. L. MacCallum, W. F. D. Bennett, and D. P. Tieleman, "Distribution of amino acids in a lipid bilayer from computer simulations," *Biophys. J.*, vol. 94, no. 9, pp. 3393–3404, May 2008.

[123] J. Yoo and Q. Cui, "Does Arginine Remain Protonated in the Lipid Membrane? Insights from Microscopic pKa Calculations," *Biophys. J.*, vol. 94, no. 8, pp. L61–L63, Apr. 2008.

[124] L. Li, I. Vorobyov, A. D. MacKerell, and T. W. Allen, "Is arginine charged in a membrane?," *Biophys. J.*, vol. 94, no. 2, pp. L11-13, Jan. 2008.

[125] D. L. Nelson, A. L. Lehninger, and M. M. Cox, *Lehninger Principles of Biochemistry*. W. H. Freeman, 2008.

[126] J. F. Nagle and S. Tristram-Nagle, "Hydrogen bonded chain mechanisms for proton conduction and proton pumping," *J. Membr. Biol.*, vol. 74, no. 1, pp. 1–14, Feb. 1983.

[127] T. Kurokawa and Y. Okamura, "Mapping of sites facing aqueous environment of voltage-gated proton channel at resting state: a study with PEGylation protection," *Biochim. Biophys. Acta*, vol. 1838, no. 1 Pt B, pp. 382–387, Jan. 2014.

[128] T. K. Berger and E. Y. Isacoff, "The Pore of the Voltage-Gated Proton Channel," *Neuron*, vol. 72, no. 6, pp. 991–1000, Dec. 2011.

Online references:

HEKA Elektronik Dr. Schulze GmbH, Ludwigshafen, Germany, 2016. Available from: http://www.heka.com/products/products_main.html#physiol_epc10single. [26 March 2016]

Luigs & Neumann, Ratingen, Germany, 2016. Available from: http://www.luigs-neumann.com/products. [26 March 2016]

National Center for Biotechnology Information (NCBI), U.S.A., 2014. Available from: http://www.ncbi.nlm.nih.gov/nuccore/GASN01342010.1?report=genbank. [03 December 2015]

Sigma-Aldrich, 2016. Available from:
http://www.sigmaaldrich.com/catalog/product/sigma/96121229?lang=de&region=DE. [18 April 2016]

University of Washington, U.S.A., 2008. Available from:
http://evolution.genetics.washington.edu/phylip.html. [08 December 2015]

Acknowledgments

First of all, I want to thank to my parents Vilma and Gerardo, and my sister Fabiola. Without their example and support I would not have been able to reach this goal; they are always present in my thoughts.

To the guys from ICS-4: Felix, Maddalena, Hua, Verena, Rachel, Daniel, Claudia, Jan-Phillipp and Anna, for all the good moments we shared together and for their friendship.

To all workers from the Institute of Complex Systems 4 from Forschungszentrum Jülich. They were always willing to help me and made a good working environment. Special thanks to my tutor Prof. Christoph Fahlke for believing in me and giving me this opportunity.

To Prof. Henrike Heise for kindly accept to be a co-supervisor of this work.

To Prof. Thomas DeCoursey for clarifying some historic facts of the voltage-gated proton channel and for providing me a complete list of publications and other works about the topic.

To Dr. Ralf Kling for helping me with the channel´s modeling.

To my friends Rodrigo, Rebecca and Moritz. They have been my adoptive family during this adventure and their emotional backing has become indispensable. I´m lucky to have found them.

Finally, I have no words to thank to Prof. Boris Musset. For his guidance, advice, support and patience along these years. For helping me with the document review. For his friendship.

Glossary

Ala: alanine.

Arg: arginine.

Asn: asparagine.

Asp: aspartic acid.

BLAST: basic local alignment search tool.

cDNA: complementary DNA.

Cl^-: chloride ion.

Cys: cysteine.

C-terminus: carboxyl terminus.

DNA: deoxyribonucleic acid.

eGFP: green fluorescent protein.

E_a: activation energy.

E_H: Nernst potential for protons.

E_m = membrane potential.

$g_{H,\,max}$: maximal proton conductance.

$g_{H,\,max}/10$: 10 % of the maximal proton conductance.

Gln: glutamine.

Glu: glutamic acid.

HBC: hydrogen bond chain.

His: histidine.

H_V1: voltage-gated proton channel.

I_{end}: end of pulse current.

I_{max}: maximal current.

I_{tail}: tail current.

k_a: acid dissociation constant.

kH_V1: *Karlodinium veneficum* voltage-gated proton channel.

LJP: liquid junction potential.

mRNA: messanger RNA.

NpH_V1: *Nicoletia phytophila* voltage-gated proton channel.

pH_i = intracellular pH.

pH_o = extracellular pH.

PCR: polymerase chain reaction.

pI: isoelectric point.

PIE: polyethylenimine.

PtH_V1: *Phaeodactilum tricornutum* voltage-gated proton channel.

NCBI: National Center for Biotechnology Information, U.S.A.

N-terminus: amino-terminus.

Q_{10}: temperature coefficient.

RNA: ribonucleic acid.

ROS: reactive oxygen species.

RT-PCR: reverse transcriptase - polymerase chain reaction.

R1, R2, R3: first, second and third arginine on S4 respectively.

Ser: serine.

S1, S2, S3, S4: first, second, third and fourth transmembrane segments respectively.

Thr: threonine.

Tyr: tyrosine.

TMA: tetramethylammonium.

Trp: tryptophan.

TSA: transcriptome shotgun assembly.

τ_{act}: activation kinetics.

U.V.: Ultra violet.

V_{hold}: holding potential.

V_{memb}: membrane potential.

V_{rev}: reversal potential.

V_{test}: test pulse potential.

V_{thres}: threshold potential.

VSD: voltage-sensing domain.

VSOP: voltage-sensor domain only protein.

VSP: voltage sensing phosphatase.

WT: wild type.